The skull of Cyclura carinata (Squamata: Iguanidae) (#94618)

First submission

Guidance from your Editor

Please submit by **10 Feb 2024** for the benefit of the authors (and your token reward) .

Structure and Criteria
Please read the 'Structure and Criteria' page for general guidance.

Raw data check
Review the raw data.

Image check
Check that figures and images have not been inappropriately manipulated.

If this article is published your review will be made public. You can choose whether to sign your review. If uploading a PDF please remove any identifiable information (if you want to remain anonymous).

Files

Download and review all files from the materials page.

23 Figure file(s)
2 Table file(s)

Structure and Criteria

Structure your review

The review form is divided into 5 sections. Please consider these when composing your review:

1. **BASIC REPORTING**
2. **EXPERIMENTAL DESIGN**
3. **VALIDITY OF THE FINDINGS**
4. General comments
5. Confidential notes to the editor

You can also annotate this PDF and upload it as part of your review

When ready submit online.

Editorial Criteria

Use these criteria points to structure your review. The full detailed editorial criteria is on your guidance page.

BASIC REPORTING

- Clear, unambiguous, professional English language used throughout.
- Intro & background to show context. Literature well referenced & relevant.
- Structure conforms to PeerJ standards, discipline norm, or improved for clarity.
- Figures are relevant, high quality, well labelled & described.
- Raw data supplied (see PeerJ policy).

EXPERIMENTAL DESIGN

- Original primary research within Scope of the journal.
- Research question well defined, relevant & meaningful. It is stated how the research fills an identified knowledge gap.
- Rigorous investigation performed to a high technical & ethical standard.
- Methods described with sufficient detail & information to replicate.

VALIDITY OF THE FINDINGS

- Impact and novelty not assessed. *Meaningful* replication encouraged where rationale & benefit to literature is clearly stated.
- All underlying data have been provided; they are robust, statistically sound, & controlled.
- Conclusions are well stated, linked to original research question & limited to supporting results.

Standout reviewing tips

The best reviewers use these techniques

Tip	*Example*
Support criticisms with evidence from the text or from other sources	*Smith et al (J of Methodology, 2005, V3, pp 123) have shown that the analysis you use in Lines 241-250 is not the most appropriate for this situation. Please explain why you used this method.*
Give specific suggestions on how to improve the manuscript	*Your introduction needs more detail. I suggest that you improve the description at lines 57- 86 to provide more justification for your study (specifically, you should expand upon the knowledge gap being filled).*
Comment on language and grammar issues	*The English language should be improved to ensure that an international audience can clearly understand your text. Some examples where the language could be improved include lines 23, 77, 121, 128 – the current phrasing makes comprehension difficult. I suggest you have a colleague who is proficient in English and familiar with the subject matter review your manuscript, or contact a professional editing service.*
Organize by importance of the issues, and number your points	*1. Your most important issue* *2. The next most important item* *3. …* *4. The least important points*
Please provide constructive criticism, and avoid personal opinions	*I thank you for providing the raw data, however your supplemental files need more descriptive metadata identifiers to be useful to future readers. Although your results are compelling, the data analysis should be improved in the following ways: AA, BB, CC*
Comment on strengths (as well as weaknesses) of the manuscript	*I commend the authors for their extensive data set, compiled over many years of detailed fieldwork. In addition, the manuscript is clearly written in professional, unambiguous language. If there is a weakness, it is in the statistical analysis (as I have noted above) which should be improved upon before Acceptance.*

The skull of Cyclura carinata (Squamata: Iguanidae)

Chloe Lai [Corresp., 1], **Simon G. Scarpetta** [1, 2]

[1] Museum of Vertebrate Zoology, University of California, Berkeley, Berkeley, Califiornia, United States

[2] Department of Environmental Science, University of San Francisco, San Francisco, California, United States

Corresponding Author: Chloe Lai
Email address: chloeemme@berkeley.edu

We provide a detailed and first description of the skull, hyoid apparatus, and trachea of the Turks and Caicos rock iguana, Cyclura carinata (Squamata: Iguanidae). Cyclura are a radiation of iguanas that are restricted to the Caribbean islands and that have high rates of endemism, and all species are severely threatened with extinction. Our anatomical description of this threatened iguana is based on high-resolution computed tomography scans of one adult, one putative adult or near adult, and one juvenile specimen, and includes three-dimensional segmented renderings and visualizations. We discuss some observations of intraspecific and ontogenetic variation, and provide a brief comparison with another species of Cyclura that was available to us. Our study provides a cranial osteological framework for Cyclura and augments the body of knowledge on iguana anatomy generally. Finally, we posit that our description and future studies will facilitate identification of fossil Cyclura, which will help understand the paleobiogeography of the genus.

The Skull of *Cyclura carinata* (Squamata: Iguanidae)

Chloe E. Lai[1], Simon G. Scarpetta[1,2]

[1] University of California, Berkeley, Museum of Vertebrate Zoology, Berkeley, California, United States
[2] University of San Francisco, Department of Environmental Science, San Francisco, California, United States

Corresponding Author:
Chloe E. Lai[1]
MVZ
Email address: chloeemme@berkeley.edu

Abstract

We provide a detailed and first description of the skull, hyoid apparatus, and trachea of the Turks and Caicos rock iguana, *Cyclura carinata* (Squamata: Iguanidae). *Cyclura* are a radiation of iguanas that are restricted to the Caribbean islands and that have high rates of endemism, and all species are severely threatened with extinction. Our anatomical description of this threatened iguana is based on high-resolution computed tomography scans of one adult, one putative adult or near adult, and one juvenile specimen, and includes three-dimensional segmented renderings and visualizations. We discuss some observations of intraspecific and ontogenetic variation, and provide a brief comparison with another species of *Cyclura* that was available to us. Our study provides a cranial osteological framework for *Cyclura* and augments the body of knowledge on iguana anatomy generally. Finally, we posit that our description and future studies will facilitate identification of fossil *Cyclura*, which will help understand the paleobiogeography of the genus.

Introduction

Morphological data from the vertebrate skeleton provide a wealth of information for biological research. Osteological data are used to understand ecomorphology (Watanabe et al. 2019), species delimitation (Keogh et al. 2008), phylogeny (Gauthier et al. 2012; Simoes et al. 2018), and pathology (Rothschild et al. 2012). Skeletal data also inform on adaptive capacity in novel situations, such as newly colonized environments and anthropogenic climate change, which has been studied in lizards (Winchell et al. 2022).

Lizards and snakes are an exceptionally diverse vertebrate radiation containing over 11,000 extant species (Reptile Database 2023). However, there is a scarcity of documented skeletal data for many lizards (Bell and Mead 2014; Evans 2008). In particular, patterns of intraspecific variation are not well understood for many squamate taxa, but there are also many species for which any detailed skeletal information is deficit or lacking entirely. Documenting intra and interspecific variation is necessary for a comprehensive understanding of species ecology, morphology, and for identifying fossils (Ledesma et al. 2021; Ledesma et al. 2023). Data from the skull are particularly important, because cranial morphology contains unique ecological information (e.g., cranial kinesis, diet) and fossil skull elements are often recovered and identified by paleontologists.

Iguanas and chuckwallas (Squamata: Iguanidae) are a group of large and generally herbivorous lizards that inhabit North, Central, and South America, the Galápagos Islands, the Caribbean islands, and the South Pacific islands of Fiji and Tonga (Buckley et al. 2016). Because of their large size, recognizability, and diversity of adaptations, iguanas are marquee components of the ecosystems they inhabit. The osteology of iguanid lizards has been studied previously, often in a systematic context (Avery and Tanner 1971; de Queiroz 1987; González Rodríguez et al. 2023, Oelrich 1956; Paparella and Caldwell 2021). Iguanas of the genus *Cyclura*, often called cycluras or rock iguanas, are especially robust, terrestrial lizards that are restricted to the Greater Antillean islands of the Caribbean Sea (Iverson 1979). Sympatry among species is uncommon, and each species for the most part solely occupies its own island and/or island bank. In part due to their restricted range size, hunting, and collection for the pet trade (Alberts 2001; Buckley et al. 2016), *Cyclura* are among the most endangered lizards on the planet. All species have a minimum IUCN Red List status of Vulnerable, many species and subspecies are Endangered or Critically Endangered (Buckley et al. 2016; IUCN 2023), and there is one described extinct species (Powell 2000). Research and especially conservation efforts have greatly increased during the 21st century, but many basic aspects of the biology of *Cyclura* are yet unknown.

Specifically, very few efforts have been made to document the skull anatomy of *Cyclura* (González Rodríguez et al. 2023) and none have been made to describe and figure in detail the anatomical features of each cranial element.

Here, we provide the first detailed assessment and visualization of the skull, hyoid, and trachea of any species of *Cyclura*. We leveraged computed-tomography scans (CT) to visualize the skulls of our focal species, *Cyclura carinata* (Turks and Caicos rock iguana). *Cyclura carinata* is restricted to the Turks and Caicos island bank and is currently considered Endangered by the IUCN Red list (Gerber et al. 2020). The total population of the species is roughly 30,000 (Gerber et al. 2020). *Cyclura carinata* is one of the smaller members of the genus (~35 cm snout to vent length), which has allowed them to persist on relatively small island cays but has also increased their vulnerability to invasive mammalian predators (Gerber et al. 2020).
We base our anatomical descriptions, images, and analyses on three specimens, so our description is relatively preliminary. That said, we provide preliminary ontogenetic data and detailed and high-resolution figures and insights into previously undescribed morphological features of *Cyclura* (e.g., the trachea). This work will provide the foundation for future investigations into the osteology of *Cyclura* and will serve as an anatomical reference for future research.

Materials & Methods

Institutional Abbreviations

UMMZ, University of Michigan Museum of Zoology; UF, Florida Museum of Natural History (University of Florida, Gainesville); MVZ, Museum of Vertebrate Zoology (Herpetology Collections)

Specimens Examined

Specimens examined via computed tomography: *Cyclura carinata*: UF Herp 32820, UMMZ 117401 (juvenile), MVZ 81381.

Traditionally prepared skeletal specimens examined for comparison. *Cyclura cornuta*: MVZ 95982 and MVZ 95983.

Computed tomography scans from three specimens of *Cyclura carinata* were examined and digitally processed to provide images of the skull, for anatomical descriptions, and for intraspecific comparisons. CT data for UF Herp 32820 and the juvenile UMMZ 117401 were obtained from Morposource.com and the specimen MVZ 81381 was CT-scanned for this project.

Ontogeny of Specimens

Complete fusion of the braincase was previously found to be indicative of sexual maturity in *Dipsosaurus* (Maisano 2002). The examined CT specimen UF Herp 32820 has near complete fusion of the braincase elements (described below), indicating sexual maturity (a proxy for adult) in both specimens. MVZ 81381 has fusion of most braincase elements so it is likely an adult or near adult, though some sutures can be seen (in particular between the prootic and the sphenoid). UMMZ 117401 is a juvenile specimen lacking fusion of any braincase element.

Information on CT Data

Specimen and scanning information are in Table 1 and anatomical abbreviations are in Table 2. We digitally segmented and disarticulated the skulls of these specimens with the software SlicerMorph in 3D Slicer (Fedorov et al. 2012; Rolfe et al. 2021) to generate digital 3D models. The digital processing consisted of image segmentations to create separate models of the skull bones for comparison. Highly fused cranial elements were not fully segmented and relative position and contact between fused elements were based on observations from existing knowledge from closely related taxa. This includes a posterior fusion of the right surangular and articular, as well as the single braincase element.

Once the CT data was loaded into 3D slicer and visible as individual slices, we adjusted the volume settings to the CT image size (0.111482 mm for UF Herp 32820). In the Segment Editor Module, we created subdivisions for the segmentations of each disarticulated cranial element. To adjust for the high intensity of the bones, the lower bounds of the density threshold range were increased such that extra pieces of cartilage or ossifications were not included in the 3D model. The draw tool was used to select large portions of the bones on the individual CT scans and the spherical paint tool was used for greater precision with smaller or articulating elements. Once applied, the selected segmentations were visible on the 3D model.

Results

General Features of the Skull

Cyclura carinata is a relatively small *Cyclura* lizard that possesses typical iguanian and iguanid features, such as a parietal foramen that is at the frontoparietal suture but mainly contained by the frontal, and a dorsal process of the squamosal (Etheridge and de Queiroz 1988). Bones are robust and well-ossified, but there is little to no rugose sculpturing on the lateral and dorsal surface of any cranial element. Some iguanids (e.g., *Conolophus*) have pronounced rugosities on their bones (Paparella and Caldwell 2021). The orbit is large and the snout is fairly elongate. Most of the teeth are multicuspid as in most other iguanids (de Queiroz 1987; Etheridge and de Queiroz 1988; Smith 2009).

MANDIBLE

The mandible consists of the dentary, coronoid, splenial, angular, surangular, and articular (Fig 6A and 6B). Some of these bones are fused, almost indistinguishably (e.g., the surangular and articular) whereas others retain clear sutural boundaries.

Dentary

The dentary is a long, robust bone located in the anterior portion of the lower jaw (Fig 2 and 4). The posterior end is taller than the anterior end and has three separate processes. The three processes articulate with the coronoid, articular, and surangular. The surangular process (posterolateral process) contacts the surangular medially while the angular process (posteroventral process) contacts the angular ventrally (Fig 6A and 6B). The shallow facet that separates the posterodorsal and surangular processes contacts the lateral process of the coronoid laterally; the lateral process of the coronoid lays on the coronoid facet of the dentary (Fig 4C). When the jaw is closed, dentary teeth stand just medial to the maxillary teeth. The Meckelian fossa of the dentary is fused for much of its length and opens anteriorly, ventral to the

mandibular symphysis (Fig 4A). Posteriorly, it is filled by the splenial and coronoid. The anterior inferior alveolar foramen is ventrally bordered by the splenial and dorsally bordered by the subdental shelf of the dentary (Fig 4B).

Large nutrient foramina appear laterally on the anterior half of the dentary and pierce into the Meckelian fossa. The right dentary has seven nutrient foramina while the left dentary has four larger nutrient foramina (Fig 4C).

Coronoid

The coronoid is a quadradiate bone consisting of three processes that articulate with the mandible and a large coronoid process (dorsal process). The coronoid contacts the dentary anteriorly, the splenial anteroventrally, and the fused articular and surangular posteroventrally (Fig 2 and 6A).

The tall, thin coronoid process is mediolaterally compressed as the body tapers to a round dorsal surface (Fig 5B). It projects dorsally and slightly angles posteriorly (Fig 5A). The process contacts the surangular posteroventrally, and clasps the posterior end of the dentary as the ventral coronoid process slots into the coronoid facet of the dentary. The long anteromedial process extends anteriorly to articulate dorsally with the dentary and ventrally with the articular, surangular, and splenial. The process extends anteriorly and ventral to the posterior end of the subdental shelf, reaching the third to last tooth position on the dentary. The anterior process narrows as it enters the posterior opening of the Meckelian fossa. The long posteromedial process is bifurcated and extends ventrally and posteriorly to articulate with the facets on the articulat and surangular, respectively. The posterior process splits into two relatively big projections and one small, middle projection.

A prominent adductor crest runs along the posteromedial margin of the coronoid process to the ventral end of the posteromedial process. The crest slightly flattens as it reaches the end of the ventral process (Fig 5A). The coronoid bears two shallow foramina located dorsomedially on the posteromedial process and medial to the adductor crest.

Splenial

The splenial is a thin bone that extends anteriorly into the Meckelian fossa. The splenial articulates with the dentary, angular, coronoid, and articular bones. The bone extends posteriorly to the midpoint of the coronoid and extends anteriorly to reach just below tooth position 14 of the dentary (Fig 6A). The anterior process of the splenial runs under the subdental shelf, tapering to a sharp tip. The anterior end of the bone contributes to the ventral border of the anterior inferior alveolar foramen. The anterior mylohyoid foramen pierces the splenial posteroventral to the anterior inferior alveolar foramen (Fig 6A). The anterior mylohyoid foramen is approximately half the size of the anterior inferior alveolar foramen and more oval-shaped.

The splenial expands posteriorly into two processes. The posteroventral process is much longer than the posterodorsal process and fits in between the angular and articular. It tapers dorsoventrally to a sharp tip. The posterodorsal process slots into a facet of the anteromedial process of the coronoid.

Angular

The angular is an elongated bone that curves along its ventral margin, forming much of the ventral border of the mandible. It is characterized by anterior and posterior processes that both taper into sharp ends. The angular contacts the fused articular and surangular bone posterodorsally, the dentary ventrally, and the splenial anterodorsally (Fig 6A and 6B).

Anteriorly, the angular underlies the posteroventral process of the splenial and contributes to the posterior region of the Meckelian fossa. In ventral view, the angular anteriorly separates into two long processes that create a v-shaped facet for the angular process of the dentary. The posterior process underlies the articular and slightly overlaps the posterolateral face of the surangular. The angular is pierced medially by the posterior mylohyoid foramen (Fig 6A).

Articular and Surangular

The articular and surangular are fused elements that form the posterior portion of the mandible. The suture of the two bones is visible medially in the segmented model, but the bones are indistinguishably fused posteriorly. Anteriorly, the broad dentary process extends past the anterolateral process of the coronoid. Together, the fused articular and surangular contact the angular ventrally, the coronoid anterodorsally and medially, the dental anteriorly, the splenial anteromedially, and the quadrate posterodorsally (Fig 6A and 6B).

On the medially curved surangular, there is a large facet for articulation with the medial processes of the coronoid and the anterior process of the articular (Fig 7B). The surangular tapers anteriorly into a bifurcated end that contributes to the posterolateral border of the Meckelian fossa. A deep adductor fossa is bounded by the surangular and articular, and opens posteriorly (Fig 7B). From the posterior end of the surangular, a prominent lateral adductor crest extends anteroventrally onto the angular (Fig 7A). The articular and surangular are completely fused just posteroventral to that crest.

In medial view, the articular tapers from the large retroarticular process to the thin anterior process. The articular also extends anteriorly to a bifurcated end that inserts into the Meckelian fossa, contacting the splenial medially and the angular both ventrally and laterally. A large depression on the dorsal surface of the retroarticular process meets the posterior end of the surangular (Fig 7B). The retroarticular process expands into a posterior knob-shaped projection and an angular process. There is a small facet that receives the mandibular condyle of the quadrate dorsally (Fig 7C). Just posterior to the condyle facet, a foramen pierces the dorsal surface of the retroarticular process for the chorda tympani branch of the facial nerve (Porter 2015). Both the anterior and posterior surangular foramina are located on the lateral face, but only the anterior foramen pierces the surangular to form a large medial opening (Fig 7A and 7B). A wide septum divides the anterior foramen. The septum is more noticeable on the left surangular compared to the right surangular.

Dentition

Cyclura carinata possesses pleurodont dentition. There are visible and deep resorption pits at the tooth bases for replacement that are located directly medial to the teeth (Fig 4B and 9B). The teeth project dorsally or ventrally and exhibit flared crowns. The teeth are also generally multicuspid with a taller, well-developed middle cusp; the teeth become increasingly unicuspid and conical distally along the tooth row (Fig 9A). The tooth height is mainly uniform but decreases distally, especially on the maxillary teeth (Fig 9A). There are 3 teeth on each side of the premaxilla with a single, small medial tooth in the process of being replaced (Fig 8A). Both maxillae have filled tooth positions and bear 20 teeth. Each dentary has 21 teeth while each maxilla has 20 teeth. There are 6 to 7 pterygoid teeth on each pterygoid (Fig 17A). Palatine teeth are absent and there no tooth positions (Fig 3B).

Premaxilla

The premaxilla forms the anterior ~~wall~~ of the skull and curves posterolaterally and posterodorsally. The body of the premaxilla is widest anteriorly at the midpoint of the alveolar plate, from which the premaxillary teeth protrude ventrally (Fig 8A). The long nasal process contributes to the anterodorsal surface of the skull and narrows posteriorly to a point as the lateral sides bear facets to contact the nasal anteriomedial processes (Fig 1). The lateral facet of the maxillary process extends posteroterally to articulate with the anterior process of the maxilla. The anterior portion of the premaxilla protrudes laterally and anteriorly past the lower jaw. Anterior premaxillary foramina are visible dorsally along the anterior surface, four of which pierce through to connect with the medial ethmoidal foramen (Fig 8A and 8C).

Maxilla

The maxilla is a large, triradiate bone that forms the posterior portion of the upper jaw (Fig 2). Both maxillae hold 20 teeth. The maxilla consists of a short premaxillary process (anterior process), a long jugal process (posterior process), and a large facial process (dorsal process). The rounded maxillary shelf flattens medially along the premaxillary process, which is short and blunt in lateral view. The premaxillary process curves medially, widening into anteromedial and anterolateral processes (Fig 9C). The bifurcated end sits on top of the medial and lateral facets of the palatal process. The anteromedial process inserts between the palatal process of the premaxilla and the anterolateral face of the vomer. Although the vomer and maxilla do not contact each other, there are articulation facets that suggest the presence of soft tissue between the two bones. The tall facial process curves dorsomedially to contribute to the anterior skull roof. The process is located slightly anterior to the midpoint of the maxilla (Fig 9A). Dorsally, the facial process narrows to a V-shaped end that inserts between the nasal and prefrontal bones. The anterior edge of the facial process contacts the lateral process of the nasal, whereas the posterior edge contacts the anteroventral process of the prefrontal (Fig 2). Just ventral to the prefrontal facet, a shallow lacrimal notch receives the anterior end of the lacrimal. The jugal process measures about one-third of the maxilla and carries most of the maxillary teeth (8 to 10 teeth). The jugal process underlies the jugal along its length, tapering posterodorsally to a sharp point (Fig 9A).

The superior alveolar canal runs along the maxillary shelf, deepening anteriorly under the facial process (Fig 9B). The large dorsal opening of the canal is visible just anterior to the facial process and is almost as wide as the premaxillary process itself (Fig 9C). The small subnarial foramen is located medial to the crista transversalis and just anterior to the dorsal opening of the superior alveolar canal (Fig 9C). Large nutrient foramina are aligned along the lateral face of the maxilla and pierce into the superior alveolar canal. The right maxilla has seven nutrient foramina and the left maxilla has nine. Additional small foramina are located irregularly on the lateral surface of the maxilla, only a few of which pierce the facial process (Fig 9A).

Nasal

The nasal is a paired bone that contributes to the anterodorsal margin of the skull. The nasals meet medially along the midbody of the two bones, diverging both anteriorly and posteriorly. Anteriorly, the nasals diverge laterally to form two separate processes: an anteromedial process that meets the premaxilla medially, and an anterolateral process (supranarial process of Gauthier et al.) that meets the maxilla ventrolaterally (Fig 1 and 2). The anterior processes exhibit a greater degree of divergence because the distance between the anterior processes is much larger than that of the posterior processes. The anterior processes narrow anteriorly and the posterior

processes narrow posteriorly; however, the tips of the anterior processes taper into narrower, sharper points than do the posterior processes (Fig 10A).

The posterodorsal face of the nasals is relatively flat, sloping anteroventrally along the anterior processes. The anteromedial processes are medially bounded by the lateral walls of the premaxilla nasal process. The anterolateral process slopes ventrally to articulate with the anterodorsal surface of the maxillary facial process and contacts the prefrontal.

At its midbody, the nasal articulates with the prefrontal posteriorly and borders the anteromedial margin of the prefrontal laterally. The posterior process flattens posteriorly and rests on top of the anterodorsal facets on the frontal.

A short, sharp anteriomedial process of the frontal slots into the space between the posteromedial borders of the nasals formed from the divergence of the two (Fig 10A). The distribution of the foramina visible on the dorsal surface is mostly random, except for the three lateral foramina located in a line along the anterolateral process (Fig 10A).

Frontal

The frontal is a long bone that contacts the nasals anteriorly and widens posteriorly to meet the parietal, contributing to the dorsal border of the skull and orbital (Fig 1). The anterior region of the frontal bone widens slightly to form a triradiate anterior that consists of two lateral and one medial process that each narrows to a point. The space between the anterior processes forms facets on which the nasal posterior processes sit (Fig 11A). The anteromedial process is short and sharp, whereas the anterolateral processes are slightly rounder at the tips. In addition, anterolateral processes slightly flare mid-length before ultimately narrowing into a tip (Fig 11A). Alternatively, the posterior processes narrow into much sharper tips than those of the anterolateral processes. The posterior region of the frontal diverges laterally into two posterolateral processes as it widens about twice the width of the anterior region. The posterior processes elongate laterally to overlap the medial process of postfrontal, extending past the lateral bounds of the anterolateral processes (Fig 11A and 11B).

The frontal meets the anterior edge of the parietal along the entirety of the posterior margin (Fig 12A). This posteromedial protrusion extends posteriorly as two short, separate projections that converge medially, enclosing the parietal foramen (Fig 11A). The posteromedial protrusion contributes to the triradiate anteromedial border of the parietal, resulting in an indent on each side of the protrusion.

Parietal

The parietal is composed of two anterior and two posterior processes that extend distally from a rectangular, dorsal midbody. Located posteriorly on the skull, the parietal contributes to the posterodorsal roof of the skull and dorsal border of the upper temporal fenestra (Fig 1). The ventral surface of the parietal is concave.

The midbody of the parietal slopes slightly anteriorly, creating a shallow dorsal depression from which two anterior processes diverge laterally to form the anterior border of the parietal. The parietal table widens anteriorly, eventually diverging laterally to form the two anterior processes that articulate with the posterior edge of the frontal (Fig 12A). The posterior half of the parietal table experiences the inverse, as it narrows to meet the anterior points of the adductor crests. The descending processes located below the dorsal shelf broaden ventrolaterally to establish the lateral bounds of the midbody (Fig 12A and 12C). Nonsymmetrical foramina occupy the dorsal face of the parietal, varying in size as they spread anterolaterally (Fig 12A).

The anterior processes extend laterally while the tips curve slightly posterolaterally. The blunt, flat ends of the processes reach slightly past the posterior processes of the frontal, articulating laterally with the posterior process of the postfrontal and the dorsomedial process of the postorbital (Fig 12B). Furthermore, the anterior processes exhibit a minor ventrolateral slope, contributing to the anterodorsal bounds of the temporal region. At the frontoparietal contact, a triradiate anteromedial structure gives rise to two larger, more rounded lateral protrusions and a short, sharp medial protrusion that inserts into the posterior opening of the parietal foramen (Fig 12A).

The posterior region of the parietal contributes dorsally to the temporal and posterior regions of the skull and is mainly characterized by two long postparietal (supratemporal) processes. The anterior processes are wider than the posterior processes but much shorter. The process tapers distally and the postparietal processes extend further laterally than the anterior processes (Fig 12B). Elongating distally from the dorsal midbody, the processes curve posterolaterally and taper in width along the entire length. Along this curve, the processes twist ventromedially such that the lateral surface faces slightly dorsally (Fig 12C). The postparietal processes are pinched dorsally to form the supratemporal crest that runs along the processes, flattening just short of the straight ends of the processes. The distal end of the process meets the supratemporal.

The posterodorsal surface of the parietal contains two nuchal fossae located at the base of each postparietal process, medial to the dorsal crest of the postparietal processes (Fig 12C). The bilateral nuchal fossae are weakly developed and present as small, shallow depressions. There is a large parietal fossa located medially on the posterior wall, just ventral to the nuchal fossa. The parietal fossa deepens anteriorly into the midbody of the parietal.

Prefrontal

The prefrontal is a robust, triradiate bone that has a posteriorly extending orbital process (posterodorsal process), an anteromedial process, and a posteroventral process. Together, the processes contribute to the anterior margin of the orbital as well as to the anterior portion of the skull roof (Fig 2). The prefrontal articulates with the frontal posteromedially, the nasal anteromedially, and the palatine ventrally. Anteriorly, the ventral portion of the anteromedial process underlies the lacrimal and maxillary facial processes and the dorsal portion underlies the lateral process of the nasal (Fig 13B). The prefrontal does not contact the the jugal.

Posteriorly, the orbital process projects posterodorsally, tapering to a sharp point (Fig 13A). The orbital process is relatively flat and much longer than the other two processes. The process articulates with the frontal medially, extending along the anterolateral process of the frontal. The posteroventral process projects posteroventrally but does not extend past the end of the orbital process. The posteroventral process curves ventrolaterally to articulate with the medial shelf of the lacrimal and enclose the lacrimal foramen (Fig 13A). The end of the posteroventral process fits into a notch on the the palatine (Fig 13C). Dorsally, a prominent ridge runs along the process to form a deep medial concavity. A shallow prefrontal foramen is visible on the dorsal ridge of the posteroventral process, as well as additional small foramina on the dorsal and medial surfaces.

Lacrimal

The lacrimal is a small bone that contributes to the anteroventral border of the orbital. The anterior margin of the lacrimal has a slight dorsolateral curve, slotting into the lacrimal notch of

the maxillary facial process (Fig 14A). The lacrimal exhibits a shallow groove along the lateral face. The anterodorsal edge of the lacrimal is flat and approximately half the width of the ventral margin. There is relatively long posteroventral process that extends posteriorly to reach the entirety of the dorsal edge of the jugal anterior process (Fig 13C).

The short medial shelf of the lacrimal articulates with the anterolateral process of the palatine and the posteroventral process of the prefrontal to fully enclose the small, oval-shaped lacrimal foramen (Fig 13A). The medial shelf forms the ventral border of the foramen while the prefrontal process forms the dorsal border.

Jugal

The jugal anteriorly contributes to the ventral margin of the orbital and posteriorly contributes to the temporal region of the skull. Located laterally on the skull, the jugal contacts the maxilla anteroventrally, the lacrimal anterodorsally, the ectopterygoid ventromedially, and the postorbital posterodorsally (Fig 14A and 14B). The long posterior (postorbital) process flares laterally to the medial process of the jugal, from which the anterior process curves medially to meet the lacrimal.

In lateral view, the jugal is the widest at the midpoint, tapering both anteriorly to a flat end and posteriorly to a sharp point (Fig 14A). This ventromedial process contacts the ectopterygoid medially and is characterized by a small protrusion that angles slightly posteriorly (Fig 14B). From the ventromedial process, both the anterior and posterior processes have a shallow groove running along the medial faces. Small foramina run along the lateral face of the anterior process, nearing the ventral margin. The right jugal bear more lateral foramina on the right jugal than the left jugal.

The anterior orbital (maxillary) process is approximately the same length as the postorbital process, but much wider (Fig 14A). Extending anterodorsally, the anterior process has a flat, wide end that articulates with the ventral margin of the lacrimal. The entire anterior process ventrally articulates with the posterodorsal margin of the maxilla

On the other end, the posterior (postorbital) process extends posterodorsally to articulate with the anteroventral face of the postorbital. The postorbital process tapers as it posteriorly elongates, ending in a width approximately one-third of the anterior process width (Fig 14C).

Ectopterygoid

The ectopterygoid is a short, thick bone that extends anterolaterally to contribute to the posterolateral border of the suborbital fenestra (Fig 3A and 3B). The bone is constricted at the midpoint in dorsal view and has an anterior jugal process and a posterior pterygoid process. The jugal process is thickest posteriorly, where the lateral ectopterygoid spur articulates with the jugal, and tapers anteriorly along the ventromedial surface of the jugal (Fig 14C). A narrow facet on the ventral surface of the jugal process rests on the posterior process of the maxilla. Posteriorly, the pterygoid process is enlarged and bifurcated to clasp the ventrolateral flange of the pterygoid (Fig 14B and 16A).

Postfrontal

The postfrontal is a small, crescent-shaped bone that forms the posterodorsal margin of the orbital (Fig 1). The anteromedial process is elongated and sharper relative to the rounded posterolateral process (Fig 3). The width of the anteromedial process tapers anteriorly, and it medially borders the posterolateral corner of the frontal. The posterolateral process is a bulbous

structure that articulates with the anterodorsal face of the postorbital (Avery, 1970). The posteromedial process contributes to the upper temporal fenestra and posteriorly contacts the parietal and postorbital. Medially, the anterior process of the postfrontal underlies the frontal and parietal bones.

Postorbital

The postorbital is a long, triradiate bone that forms the posterior margin of the orbital. Dorsally, the anterior process articulates anteriorly with the postfrontal and anterolaterally with the parietal (Fig 2). The postorbital narrows posteriorly to meet the squamosal posteroventrally. The ventral face of the anteroventral process articulates with the jugal, extending anteriorly as it overlaps the posterior process of the jugal dorsomedially (Fig 14A and 14B). This jugal process is longer than the anterodorsal and posterior processes.

Squamosal

The squamosal is a small, slender bone that slopes anteroventrally. Located in the temporal region, the squamosal lies in between the postorbital, quadrate, and supratemporal bones (Fig 2). The anterior process underlies the posteroventral surface of the postorbital without contact, leaving a small gap remaining between the two bones that suggests the presence of soft tissue articulation. The posteroventral face articulates with the posterodorsal surface of the quadrate, while the small posteromedial (dorsal) process laterally articulates with the posterolateral face of the supratemporal. The posteroventral process slots into the squamosal notch on the dorsal surface of the quadrate.

Supratemporal

The supratemporal is a long, slender bone located in the posterior region of the skull that contacts the quadrate, squamosal, parietal, and braincase (i.e., the paroccipital process). The posterior process is rounded and lies in between the squamosal, postparietal process, paroccipital process, and cephalic condyle (Fig 12C). The supratemporal extends anteriorly along the medioventral face of the postparietal process, tapering to a sharp point. The rounded posterior process has a small notch that accommodates the posterior process of the squamosal. This notch creates a shallow groove that flattens along the anterior process. The medial face of the posterior process articulates with the paraoccipital process (Fig 12C). The thin dorsal surface fits in between the squamosal and paroccipital process, preventing contact between the two. The posterior process lies on top of the cephalic condyle to contact the quadrate ventrally.

Quadrate

The quadrate is a robust vertically oriented bone located in the posterior of the skull. The bone contacts the supratemporal and squamosal dorsally, the pterygoid ventromedially, and the articular ventrally (Fig 2). The quadrate is narrow ventrally and widens dorsally to form the broad, well-developed cephalic condyle, which is located dorsomedially. The cephalic condyle is slightly sloped posteroventrally and is overlapped by the squamosal anteriorly and supratemporal dorsomedially (Fig 15D). The small ventromedial knob of the squamosal fits into the squamosal notch located dorsally on the quadrate.

The column runs along the vertical length of the quadrate and is laterally bounded by a deep quadrate conch (Fig 15C). A wide flange extends medially from the column. This flange is wider and has a depression deeper than the conch. The quadrate bears a lateral tympanic crest

that thickens slightly anterior to the conch, reaching the cephalic condyle dorsally (Fig 15B). A small, shallow pterygoid lamina is present on the medial flange of the quadrate above the mandibular condyle (Fig 15C). It articulates medially with the quadrate process of the pterygoid. The mandibular condyle sits on top of the articular and is characterized by round lateral and medial condyles.

The ossification on top of the cephalic condyle forms a pitted structure. Separated by the central column, two additional foramina are present above the mandibular condyle. Both foramina pierce the quadrate and are visible on the anterior and posterior faces of the quadrate (Fig 15A and 15C). The medial foramen, however, is much larger than the lateral foramen on both faces.

Pterygoid

The pterygoid is a long, triradiate bone that is located in the posterior region of the palate (Fig 3A and 3B). The interpterygoid vacuity separates the pterygoid from its contralateral pair and the pterygoid contacts the epipterygoid dorsally, palatine and ectopterygoid anteriorly, and quadrate posterolaterally (Fig 16A and 16B).

The anterior palatine process is relatively flat dorsoventrally and thickens medially. The anterolateral margin of the process is slightly concave and laterally contributes to the posteromedial border of the suborbital fenestra (Fig 16A). In dorsal view, the palatine process expands anteriorly to slot into the dorsal pterygoid facet of the palatine. A small notch on the dorsal surface of the palatine process of the pterygoid receives the posterolateral projection of the palatine (Fig 17A). A small anterior foramen is present on the shallow dorsomedial groove of the palatine process. The pterygoid expands ventrally from the midpoint of the bone into a short ventromedial flange and a larger ventrolateral flange (transverse process). The small ventromedial flange is rounded along its medial edge and has a thin dorsal groove that bears a foramen that pierces it medially. The ventrolateral pterygoid flange is curved anterolaterally and has an expanded, notched end that forms a joint articulation with the posterior process of the ectopterygoid (Fig 16A). An additional large foramen is visible on the dorsal surface, just anterior to the ectopterygoid facet. Dorsal to the ventromedial pterygoid flange, there is a small dorsal facet that receives the ventral end of the ecotopterygoid. The fossa columella opens dorsally at the base of the posterior quadrate process of the pterygoid (Fig 17B). The elongate quadrate process extends posterodorsally to articulate with the pterygoid lamina of the quadrate. At the base of the process, a short ridge forms on the dorsal surface just dorsal to the fossa columella.

Small pterygoid teeth are present on the ventromedial face of the palatine process, all of which are similar in size and conical shape (Fig 16A and 17A).

Epipterygoid

The epipterygoid is a long, cylindrical bone that extends dorsally from the fossa columella of the pterygoid towards the epipterygoid process of the parietal. The epipterygoid is slightly inclined posterodorsally and is laterally convex at the midpoint. The dorsal end is mediolaterally compressed. A shallow groove widens along the ventrolateral surface of the epipterygoid and is anteroposteriorly compressed. The epipterygoid does not reach the descending (epipterygoid) process of the parietal, leaving a large dorsal gap between the two bones. The rounded, ventral end of the epipterygoid fits into the fossa columella of the pterygoid (Fig 17B).

Septomaxilla

The septomaxilla is a thin paired bone located in the vomeronasal region, just posterior to the premaxilla and dorsal to the vomers. A small medial space that is widened anteriorly separates the septomaxillae. The septomaxilla is characterized by its tapering anterior process, broad dorsal process, and small ventral projection. In dorsal view, the bone is horizontally oriented, whereas the posterior half of the septomaxilla is steeply inclined toward the skull roof (Fig 18A).

The anterior end tapers to a point and curves medially along the medial margin of the anterior process of the maxilla. The right septomaxilla has a more distinct articulation with the maxilla while the left maxilla has a left small gap between the two, suggesting intraspecific variation. The septomaxilla is laterally constricted, forming a short dorsal ridge and a small lateral notch (Fig 18A). Viewed anteriorly, the posterior process is both medially and laterally raised into tall walls that form a deep dorsal groove. This dorsally projecting process thickens posteriorly before ending in a short point. At the midpoint of the septomaxilla, a ventral process projects from the lateral margin to contact the dorsolateral surface of the vomer (Fig 18B). A shallow groove widens posteriorly on the ventral surface of the posterior process. There are small, randomly placed foramina on the dorsal surface of the septomaxilla.

Vomers

The vomers are short, paired bones that are located ventral to the septomaxilla and form the anterior portion of the palatal bones. The vomers taper anteriorly to a point, contacting each other medially along most of their length, and widen posteriorly to contact the palatines dorsally (Fig 3A). A short medial process protrudes from the anterior end of the left vomer and fits into a facet on the right vomer.The small, deep vomeronasal region of the vomer sits just posterior to this anteromedial process and lateral to a medial crest. The tall medial crest runs along the vomer, forming a dorsal groove that widens posteriorly and a large facet that clasps the vomerine process of the palatine (Fig 3A). The medial surface is pierced by small foramina that are not visible when the vomers are in articulation. Large foramina that occupy the dorsal groove are visible along the ventral surface of the vomer, including the foramen for the medial palatine nerve. An additional medial foramen located in the vomeronasal region pierces the bone, opening on the ventromedial margin. A raised anterolateral shelf extends from the vomeronasal region, separating the nasal region from the choana. On the ventral surface, a sharp ridge curves posterolaterally from the anterior tip to join the lateral crest of the vomer (Fig 3B).

Palatine

The palatines are large, paired bones located between the vomer and pterygoid palatal bones (Fig 3A and 3B). The palatine has a ventrally sloped pterygoid process, a vomerine process, and two laterally projecting maxillary processes.

Anteriorly, the vomerine process tapers to slot into a large facet on the posterior process of the vomer. A thin crest extends from the medial crest of the vomer, forming a deep dorsal groove along the vomerine process to the base of the maxillary processes (Fig 16B). There are small protrusions along the posteromedial margin of the vomerine process that indicate articulation with the vomer. A deep choanal groove is present on the ventral surface of the palatine (Fig 16A). Two short maxillary processes project laterally to articulate with the maxilla, the prefrontal and lacrimal dorsally, and the jugal laterally. The medial shelf of the lacrimal and the posteroventral process of the prefrontal fit into a dorsal depression on the dorsolateral process of the palatine. The ventrolateral process articulates with a facet on the medial surface of the

jugal and sits on the posterior end of the maxillary shelf. The posterior pterygoid process is dorsoventrally flattened and narrows posteriorly to a bifurcated end with short medial and lateral projections (Fig 16B). The posterior end has a dorsal facet that accommodates the anterior process of the pterygoid and a lateral projection that fits into a dorsal notch on the pterygoid. The ventrolateral process and posterior pterygoid process contribute to the anterior and medial borders of the suborbital foramen (Fig 3B and 16B).

The infraorbital foramen opens anteriorly through the ventrolateral maxillary process, just above the maxillary shelf (Fig 16B). Aligned along a shallow, dorsal depression on the pterygoid process, multiple small foramina pierce the palatine and are visible ventrally. Additional foramina occupy the vomerine process along the anteromedial crest and open medially into the space between the palatines. A small foramen is present on the dorsal surface of the dorsolateral process, just ventral to the articulation of the prefrontal. There are no palatal teeth present on the ventral surface.

Stapes

The stapes is a thin, cylindrical bone that slightly slopes ventrally as it extends posterolaterally from the braincase (Fig 19B and 21B). Although both ends are expanded, the stapes is thickest at the round medial end. The medial end of the stapes is in the fenestra ovalis, whereas the lateral end extends into the space posterior to the quadrate (Fig 21A). There are two isolated ossifications just posterior to each stapes. These fragments are present on both sides and extend along the same direction of the stapes, tapering to a small point.

Orbitosphenoid

The orbitosphenoid is a paired, ossified element that is isolated from the other cranial bones. The orbitosphenoid forms from the ossification of the orbitotemporal cartilages pila metoptica and taenia medialis (Tarazona 2008). Compressed dorsoventrally, the orbitosphenoid is located dorsal to the parasphenoid process. The orbitosphenoid extends anterodorsally towards the roof of the skull and the ends of the bone curve medially, forming a triradiate shape.

BRAINCASE

General features of the braincase

The braincase of *Cyclura carinata* is a posterior structure of the skull that articulates with the vertebral column via the occipital condyle (Fig 19B). It is defined by five main elements: the anteroventral sphenoid, the posteroventral basioccipital, the dorsal supraoccipital, the paired lateral prootic, and the paired posterior otooccipital. Together, the elements possess articulations with the pterygoids, the stapes, the quadrate, the supratemporal, and the postparietal processes of the parietal. The otooccipital is defined by a fusion of the exoccipital and the opisthotic elements. The fusion between the bones forms large foramina, including the posterior foramen magnum and fenestra ovalis (Fig 19B). Although the bones are separate elements, sutures are not clearly distinguishable for UF Herp 32820 indicating complete fusion of the braincase. Most of the braincase is fused in MVZ 81381 besides the prootic and the sphenoid, and UMMZ 117401 lacks braincase fusion.

Supraoccipital

The dorsal roofing of the braincase is formed by the supraoccipital, which also borders the foramen magnum dorsally. The supraoccipital meets the prootic ventrally and anterolaterally and

meets the otooccipital posteriorly (Fig 19A). The supraoccipital is concave in lateral view. Lateral flanges of the supraoccipital are triangular in shape and slope ventrally to slightly overlap the otoocipital.

The processus ascendens is short and broad in dorsal view and has two small lateral projections. The processus ascendens extends anteriorly to approach the deep parietal fossa but does not establish contact with the parietal. A weak midsagittal crest forms posteriorly on the dorsal surface of the processes ascendens (Fig 19B). The dorsal surface is occupied by two wide, shallow depressions on both sides of the processes ascendens. Along the posterior edge, there is a prominent notch at the midline of the supraoccipital (Fig 19A).

The lateral flange of the supraoccipital contributes to the dorsomedial roof of the cavum capsularis. The small groove of the utricular recess runs along the internal medial surface of the cavum capsularis, just dorsal to the osseous common crus. From the cavum capsularis, the large common crus deepens anteriorly to merge with the anterior and posterior semicircular canals (Villa et al. 2018). The anterior semicircular canal opens dorsally from the anterior ampullar recess towards the articulation of the supraoccipital and prootic, and the posterior semicircular canal opens posterolaterally towards the otooccipital (Fig 21A). The small endolymphatic foramen is located in the cavum capsularis, just lateral to the osseous common crus (Oelrich 1956). It pierces the supraoccipital anteromedially and opens as a narrow foramen on the external medial surface of the supraoccipital.

Basioccipital

The basioccipital forms the posteroventral floor of the braincase as well as the ventral and medial portions of the occipital condyle. The basioccipital contacts the otooccipital and prootic dorsally, the sphenoid anteriorly, and the atlas vertebra posteriorly (Fig 19A and 19B). The basioccipital is anteriorly fused to the sphenoid, and there is no distinguishable suture visible on the ventral surface. The dorsal surface is concave and widest at the midpoint of the bone. The posterior half of the basioccipital tapers and projects posterodorsally. Small basal tubercles extend ventrolaterally into rounded ends, forming a deep groove on the ventral surface. Only the juvenile *Cyclura carinata* specimen UMMZ 117401 has paired on the ventral surface, medial to the basal tubercles. The thin crista interfenestralis extends along the anterodorsal face of the basal tubercles, wh also contributes the ventral border of the lateral aperture of the recessus scalae tympani (Fig 21B).

Sphenoid

The sphenoid forms the anteroventral portion of the braincase and features a parasphenoid process and a fused parasphenoid and basisphenoid (Fig 19A and 21A). The sphenoid contacts the basioccipital posteriorly and the prootic dorsolaterally. The short alar processes project anteriorly from the dorsal surface and slightly narrow into rounded ends (Fig 21A). Medial to the alar processes, a small dorsum sella projects anteriorly and provides to the posterodorsal border of the pituitary fossa (Fig 20A). The pituitary fossa is deeply concave and opens anteriorly. The abducens foramen pierces the medial wall of the pituitary fossa and opens on the dorsal surface, just posterior to the crista sellaris (Fig 20A and 20B). The anterior vidian canal opening is present posterolateral to the trabecula and ventral to the abducens foramen. The vidian canal opens posteriorly on the lateral face of the sphenoid and is medially bordered by the prootic (Fig 21B). A thin medial septum on the posterior wall separates the internal carotid foramina and ends

posterior to the sella turcica. The internal carotid foramen merges with the vidian canal, opening posteriorly.

Medial to the trabeculae, the long parasphenoid process projects anterodorsally and tapers to a point. A thin dorsal groove slightly widens anteriorly along the process (Fig 19A). The parasphenoid elongates into the space medial to the pterygoids but does not articulate with the anterior palatine process of the pterygoid.

The basipterygoid process extends anterolaterally from the sphenoid and expands distally into rounded ends (Fig 19B and 20A). The entire basipterygoid process slots into a large medial notch on the pterygoid, just anteroventral to the postepiterygoid groove. Between the alar process and the basipterygoid process, there is a small notch that encloses the lateral head vein.

Prootic

The prootic is a paired, triradiate bone that forms the anterolateral region of the braincase. The prootic contacts the otooccipital posteriorly, the supraoccipital dorsally, the sphenoid anteroventrally, and the basioccipital posteroventrally (Fig 19A and 21A). The prootic alar process extends anterodorsally but does not anteriorly extend past the processus ascendens of the supraoccipital to contact the postparietal process. The wide incisura prootica forms along the dorsal margin of the anterior inferior process and is medioventral to the alar process and anterior ampullar recess (Fig 20B and 21A). The ampullar recess is bulbous on the lateral surface of the prootic. A thin crest extends anteriorly along the medial surface of the prootic, terminating just posterior to the small supratrigeminal process (Fig 20B).

A sharp crest runs posterodorsally from the ventral margin of the anterior inferior process to the posterior process of the prootic, forming the crista prootica (Fig 21A). The crista prootica is expanded ventrally near its midpoint, forming a round, ventrally projecting lamina. The crista prootica continues onto the posterior process of the prootic, contacting the paraoccipital process of the otooccipital posteriorly. The posterior process contributes to the anterior region of cavum capsularis, enclosing within it the anterior half of the horizontal semicircular canal. Along the ventral margin, the prootic contacts the alar process of the sphenoid to form the posterior opening of the vidian canal (Fig 21B). The posterior opening expands onto the laterally exposed groove of the recessus vena jugularis. Posterodorsal to the recessus vena jugularis is the small facial foramen (VII), which is visible medially but obscured in lateral view by the crista prootica (Fig 20B).

The medial face of the prootic has a deep pit, the acoustic recess, which is occupied by the medial openings of the large acoustic foramina and the foramen. The acoustic recess is located posterior to the incisura prootica. Dorsal to the facial foramen, the anterior acoustic foramen opens into the anterior ampullary recess while the posterior acoustic foramen opens internally into the cavum capsularis. The paths of the anterior and horizontal semicircular canals are visible as prominent ridges on the lateral surface of the prootic (Fig 21A). The anterior semicircular canal extends anterodorsally from the ampullar recess and opens at the articulation of the prootic and supraoccipital (Evans 2008). The horizontal semicircular canal opens on the posterior process of the prootic. The prootic contacts the otooccipital posteromedially to form the anterior and lateral borders of the fenestra ovalis (Fig 21B).

Otooccipital

The otooccipital contributes to the posterodorsal portion of the braincase. The otooccipital contacts the basioccipital ventrally, the supraoccipital dorsally, and the prootic anterolaterally. It

forms the posterior border of the cavum capsularis as well as the lateral borders of the foramen magnum. Ventral to the foramen magnum, the occipital condyle is composed of the medial basioccipital condyle and the triangular, dorsolateral knobs of the otooccipital (Fig 19B). The otooccipital portions of the condyle are smaller than that of the basioccipital and are slightly mediolaterally compressed. Viewed posteriorly, the paired paraoccipital processes are large and robust and extend dorsolaterally into rounded ends. These posterior ends laterally articulate with the posteromedial facet of the supratemporal, the postparietal process, and the cephalic condyle of the quadrate. A well-developed ridge runs anteromedially along the paraoccipital process and merges with the thin crista interfenestralis. From the base of the paraoccipital process, the crista interfenestralis extends ventrally to the basal tubercles, separating the external lateral opening of the fenestra ovalis and lateral aperture for the recessus scala tympani (Fig 21B).

Located dorsolateral to the crista tuberalis is the large fenestra ovalis, which is posteriorly bordered by both the otooccipital and prootic (Fig 21A and 21B). The fenestra ovalis opens posterolaterally and receives the expanded proximal end of the stapes. In anterior view, the fenestra ovalis pierces the bone medially and runs dorsolateral to the small lagenar recess. A thin medial crest of the lagenar recess bifurcates anteriorly, separating the lagenar recess from the posterior ampullar recess. Anterior to the posterior ampullar recess, a low ridge forms along the medial surface of the otooccipital as the utricular recess extends anteriorly. Ventral to the posterior ampullar recess is the perilymphatic foramen, which opens dorsal to the lagenar recess. The otooccipital contains the openings of the horizontal semicircular canal and the posterior semicircular canal at the articulations with the prootic and supraoccipital, respectively. Both semicircular canals connect anteriorly with the posterior ampullar recess.

The wide lateral aperture for the recessus scala tympani is oval in shape and is located ventral to the foramen ovalis (Fig 21B). It is bordered dorsolaterally by the crista interfenestralis and dorsomedially by the crista tuberalis, a distinct crest that extends ventrally onto the basal tubercle. There is a small foramen just ventral to the base of the paraoccipital process. The smaller, circular medial aperture of the recessus scala tympani is visible within the lateral aperture from a dorsolateral view. Dorsomedial to the lateral aperture and immediately lateral to the foramen magnum, there is a narrow pocket that is pierced by the vagus foramen (Fig 21B). The lateral end of the vagus foramen is divided by a thin septum. Three hypoglossal foramina are aligned along the posteromedial surface, just ventral to the vagus foramen (Fig 20B).

Trachea

The trachea is a long, midline structure located in the posterior region of the skull (Fig 1 and 2). It is separate from the other cranial bones and is located just posterior to the posterior ends of the dentaries (Fig 22). The trachea consists of a series of identical, cartilaginous rings that are evenly spaced and incomplete dorsally (Oelrich 1956). Dorsal to the hyoid apparatus, the trachea extends posteroventrally past the atlas and axis vertebrae.

Hyoid apparatus

The hyoid apparatus is located posteroventral to the skull and dorsal to the larynx and does not contact any other skeletal components (Fig 3). The hyoid apparatus is characterized by symmetrical, gradually tapering ossifications that extend distally from the central basihyoid. The basihyoid is a triradiate structure consisting of the long processus lingualis and the paired second ceratobranchials.

The processus lingualis projects anteriorly from the basihyoid into the interpterygoid vacuity between the pterygoids, extending just anterior to the pterygoid teeth (Fig 23B). The hyoid cornu is half the length of the processus lingualis and extends anterolaterally to the lateral processes of the pterygoids. Viewed laterally, the hyoid cornu slightly projects dorsally toward the dentaries (Fig 23A). A long, thin anteromedial foramen is fully enclosed by the anterior end of the paired epihyals, which almost articulates with the hyoid cornu. The slender epihyal extends posterolaterally past the atlas vertebra. In lateral view, the epihyal projects posteroventrally and curves dorsally at a point ventral to the braincase (Fig 23A). The posterior end tapers to a point and curves anterodorsally toward the posterior process of the articular. The paired first ceratobranchials possess knob-shaped ossifications at the anterior end that almost contact small anterolateral depressions on the second ceratobranchials. At a point ventral to the quadrate, the first ceratobranchial curves dorsally and gradually taper to a round end. The first epibranchial projects anterodorsally from the posterior end of the first ceratobranchial. The second ceratobranchials are fused to the basihyoid and extend posteriorly just ventral to the larynx. In lateral view, the second ceratobranchial projects posteroventrally along the entire length. The free epibranchial is located anteromedially to the first ceratobranchial and extends posterolaterally towards the first epibranchial (Fig 23B).

Comparison of the skulls of *Cyclura carinata* and *Cyclura cornuta*

We examined traditionally prepared skeletons of *Cyclura cornuta* to provide a comparative benchmark of the anatomy of non-CT scanned specimens of *Cyclura*, and to provide some preliminary interspecific comparisons between *Cyclura carinata* and other members of the genus. Here we also present several ontogenetic and intraspecific comparisons within *Cyclura carinata*.

Premaxilla

Both skeletal specimens of *Cyclura cornuta* bear nine teeth on the premaxilla, but the specimens of *Cyclura carinata* exhibit variation in the number of teeth. The large and presumably adult specimen UF Herp 32820 and the juvenile UMMZ 117401 possess seven teeth, whereas the large specimen MVZ 81381 has eight teeth (Fig 8A). The external nares are partly formed by the posterior margins of the premaxilla but differ in shape among examined specimens. *Cyclura carinata* UF Herp 32820 has wide external nares that do not extend posteriorly past the nasal process of the premaxilla (Fig 1 and Fig 2). The external nares of *Cyclura cornuta* and *Cyclura carinata* MVZ 81381 are narrow and more ovular in shape. In *Cyclura cornuta* MVZ 95983 and MVZ 95982, the septomaxilla anteriorly contacts the ventral surface of the premaxillary nasal process. The nasal processes of the adult specimens have a lateral flare at the midpoint of the process that the juvenile *Cyclura carinata* UMMZ 117401 lacks, suggesting an ontogenetic difference. The juvenile also lacks the anterior premaxillary foramina that are present in the adult specimens.

Maxilla

The dorsal opening of the superior alveolar canal is present in all of the adult specimens, as well as the subnarial arterial foramen. Both of the subnarial arterial foramina on *Cyclura carinata* UF Herp 32820 and *Cyclura cornuta* MVZ 95983 are small. On *Cyclura cornuta* MVZ 95982, the foramen is oval in shape and larger than the dorsal opening of the superior alveolar canal. *Cyclura carinata* MVZ 81381lacks both openings on the right maxilla, and the *Cyclura carinata*

juvenile lacks both subnarial foramina. The maxillary teeth of the juvenile *Cyclura carinata* specimen are not well-developed and do not have a prominent tricuspid shape. It also lacks the nutrient foramina along the lateral face of the maxilla.

Dentary

Specimens of *Cyclura carinata* possess multicuspid posterior teeth, as well as *Cyclura cornuta* MVZ 95983 (Fig 4B). However, the juvenile *Cyclura carinata* UMMZ 117401 is missing foramina along the lateral face of the dentary.

Nasals

The nasals of the juvenile *Cyclura carinata* UMMZ 117401 diverge posteriorly and there is a large medial gap along the posterior half of the nasals. The specimen also exhibits a large gap between the lateral margin of the nasal and the prefrontal that is absent on the adult specimens of both *Cyclura carinata* and *Cyclura cornuta.*

Frontal

Both examined specimens of *Cyclura cornuta* have long, flat frontals. In lateral view, the dorsal surface of the skull is slightly depressed from the anterior end of the frontals to the anterior tip of the parietal crest. In *Cyclura carinata* specimens, the frontals are round and the dorsal surface is slightly convex.

Parietal

The parietal descending process in *Cyclura cornuta* specimens MVZ 95983 and MVZ 95982 contact the anterior alar process of the prootic, unlike in the *Cyclura carinata* species. A tall midline crest is present on the dorsal surface of the parietal in *Cyclura cornuta* specimens. *Cyclura carinata* specimens have a more smooth dorsal surface and lack the parietal crest (Fig 12A). On this dorsal surface, the parietal foramen is present in *Cyclura carinata* UF Herp 32820 and both *Cyclura cornuta* specimens. The parietal foramen of *Cyclura cornuta* specimens are circular and fully enclosed on the dorsal surface. In *Cyclura carinata* UF Herp 32820 and MVZ 81381, the parietal foramen is ovular and narrow; there is a thin posterior opening that receives an anterior projection of the parietal (Fig 12A and 12B). The juvenile *Cyclura carinata* UMMZ 117401 does not have this small foramen, but instead exhibits a large frontoparietal fontenelle between the frontal and parietal that is almost as wide as the skull (Hernández-Jaimes et al. 2012). There are multiple foramina present on the dorsal surface of *Cyclura carinata* UF Herp 32820 and MVZ 81381 but absent on *Cyclura cornuta* specimens (Fig 12A). Instead, most of the dorsal surface of *Cyclura cornuta* is occupied by the long parietal crest. The dorsal surface of the juvenile *Cyclura carinata* is smooth and does not have any additional foramina. The parietal of the juvenile is mediolaterally constricted and does not contact the processus ascendus of the supraoccipital. Unlike *Cyclura carinata* UF Herp 32820, the parietal of *Cyclura carinata* MVZ 81381 shows a complete fusion to the supraoccipital.

Postfrontal

In both skeletal specimens of *Cyclura cornuta*, the lateral process of the postfrontal is narrow and projects anteriorly (Avery, 1970). The postfrontals of *Cyclura carinata* specimens, including the juvenile specimen, are short and project laterally, along the anterior margin of the postorbital.

Jugal

A bulbous projection on the lateral surface of the jugals is present at the midpoint of the jugals of the *Cyclura cornuta* specimens. The jugals of specimens of *Cyclura carinata* have a smooth lateral surface and lack a lateral projection (Fig 14A).

Pterygoid

On *Cyclura carinata* UF Herp 32820, the left pterygoid has six to eight pterygoid tooth positions and one empty position, whereas the right pterygoid has five teeth and two empty positions (Fig 3B and 14A). The teeth are clumped together in a pit in *Cyclura carinata* but are aligned in a row in *Cyclura cornuta* MVZ 9598. In *Cyclura carinata* MVZ 81381, the pits for the pterygoid teeth are present, but teeth are not visible on either the segmentation or the CT slices.

Quadrate

Adult specimens of *Cyclura carinata* and *Cyclura cornuta* possess ossified cartilage on top of the cephalic condyle that contributes to the tight articulation of the quadrate, the squamosal, postparietal process, and the supratemporal (Fig 15C and 15D). The calcified cartilage is not present on the quadrate of the juvenile *Cyclura carinata* UMMZ 117401.

Epipterygoid

In examined specimens of *Cyclura carinata*, the epipterygoid does not contact the descending process of the parietal. However, the dry skeletal specimens of *Cyclura cornuta* MVZ 95983 and MVZ 95982 exhibit contact between the parietal and epipterygoid or the two elements are in much closer proximity than in the CT-scanned specimens, which is very likely due to the preservation mode of the skeletal specimens. We suggest that shrinking of soft-tissue during skeletal preparation brings the parietal and epipterygoid into contact or close to contact.

Prootic

Cyclura carinata bears a projection at the midbody of the crista prootica along the ventral margin (Fig 21A). *Cyclura cornuta* MVZ 95983 also has this ventral projection, but it is less prominent than that of *Cyclura carinata*. *Cyclura cornuta* MVZ95982 does not possess the ventral protrusion. The prootic alar processes of all specimens do not contact the epipterygoid.

Otooccipital

The lateral opening of the vagus foramen in *Cyclura carinata* UF Herp32820 and MVZ 8138 and both *Cyclura cornuta* specimens is split into two openings by a thin septum (Fig 21B). The paraoccipital processes of juvenile *Cyclura carinata* UMMZ 117401 and MVZ 81381 are not well-developed and terminate at the articulation with the cephalic condyle.

Figure Captions

Figure 1. Dorsal view of the entire skull of *Cyclura carinata* UF Herp 32820. Scale bar = 10 mm.

Figure 2. Lateral view of the entire skull of *Cyclura carinata* UF Herp 32820. Scale bar = 10 mm.

Figure 3. Palatal bones of *Cyclura carinata* UF Herp 32820. **A** dorsal view, **B** ventral view. Scale bar = 10 mm.

Figure 4. Right dentary of *Cyclura carinata* UF Herp 32820. **A** ventral view, **B** medial view, **C** lateral view. Scale bar = 1 mm, 10 mm for reference skull.

Figure 5. Left coronoid of *Cyclura carinata* UF Herp 32820. **A** lateral view, **B** posteromedial view. Scale bar = 5 mm, 10 mm for reference skull.

Figure 6. Right mandible of *Cyclura carinata* UF Herp 32820. **A** medial view, **B** lateral view. Scale bar = 1 mm, 10 mm for reference skull.

Figure 7. Right articular and surangular of *Cyclura carinata* UF Herp 32820. **A** lateral view, **B** medial view, **C** ventral view. Scale bar = 1 mm, 10 mm for reference skull.

Figure 8. Premaxilla of *Cyclura carinata* UF Herp 32820. **A** anterior view, **B** posterior view, **C** lateral view. Scale bar = 1 mm.

Figure 9. Left maxilla of *Cyclura carinata* UF Herp 32820. **A** lateral view, **B** medial view, **C** anterior view. Scale bar = 5 mm, 10 mm for reference skull.

Figure 10. Nasals of *Cyclura carinata* UF Herp 32820. **A** dorsal view, **B** ventral view. Scale bar = 5 mm, 10 mm for reference skull.

Figure 11. Frontals of *Cyclura carinata* UF Herp 32820. **A** dorsal view, **B** ventral view. Scale bar = 1 mm, 10 mm for reference skull.

Figure 12. Frontal and Parietal of *Cyclura carinata* UF Herp 32820. **A** dorsal view, **B** ventral view. Scale bar = 10 mm.

Figure 13. Lacrimal and prefrontal of *Cyclura carinata* UF Herp 32820. **A** right prefrontal and lacrimal in posterior view, **B** right prefrontal in lateral view, **C** right lacrimal in lateral view. Scale bar = 5 mm, 10 mm for reference skull.

Figure 14. Right lacrimal, jugal, ectopterygoid, and postorbital of *Cyclura carinata* UF Herp 32820. **A** lateral view, **B** medial view. Scale bar = 10 mm.

Figure 15. Right quadrate of *Cyclura carinata* UF Herp 32820. **A** anterior view, **B** right lateral view, **C** posterior view, **D** left lateral view. Scale bar = 1 mm, 10 mm for reference skull.

Figure 16. Right palatal bones of *Cyclura carinata* UF Herp 32820. **A** ventral view, **B** dorsal view. Scale bar = 10 mm.

Figure 17. Right pterygoid of *Cyclura carinata* UF Herp 32820. **A** anterior view, **B** dorsal view. Scale bar = 10 mm.

Figure 18. Septomaxillae of *Cyclura carinata* UF Herp 32820. **A** anterior view, **B** lateral view. Scale bar = 1 mm, 10 mm for reference skull.

Figure 19. Braincase of *Cyclura carinata* UF Herp 32820. **A** dorsal view, **B** posterior view. Scale bar = 10 mm.

Figure 20. Braincase of *Cyclura carinata* UF Herp 32820. **A** anterior view, **B** anterolateral view. Scale bar = 10 mm.

Figure 21. Braincase of *Cyclura carinata* UF Herp 32820. **A** lateral view, **B** posterolateral view. Scale bar = 10 mm.

Figure 22. Trachea of *Cyclura carinata* UF Herp 32820 in posterolateral view. Scale bar = 10 mm.

Figure 23. Hyoid of *Cyclura carinata* UF Herp 32820. **A** lateral view, **B** ventral view. Scale bar = 10 mm.

Discussion

We provide the first, extensive insight into the skull, hyoid apparatus, and trachea of *Cyclura carinata*, establishing an anatomical framework for the skull of *Cyclura* and adding to the body of literature detailing the cranial osteology of extant iguanid lizards (Bochaton et al. 2016; de Queiroz 1987; Oelrich 1956; Paparella and Caldwell 2021). Through the use of CT data and processing software, we constructed a digital, three-dimensional model of the skull and its disarticulated cranial elements. The model allowed observation of the articulations and fusions between bones and provided preliminary data on interspecific variation between *Cyclura carinata* and other *Cyclura* (*C. cornuta*). We also examined some differences between CT-scanned and traditionally prepared skeletal specimens.

Morphological differences between adult and juvenile specimens, such as a large parietal opening or an underdeveloped premaxillary nasal process, indicate ontogenic traits that distinguish the adult and juvenile *Cyclura carinata*. Ontogenetic increases in cusps and size are observed between the juvenile and adult *Cyclura carinata* (de Queiroz 1987). While both the dentary and maxillary teeth of *Cyclura* specimens increase in size posteriorly, the teeth of the juvenile *Cyclura carinata* are not well-developed and are unicuspid, whereas the adult *Cyclura carinata* are multicuspid. The shape of the juvenile *Cyclura carinata* parietal is less defined compared to that of the adult specimen, and it exhibits a smooth dorsal surface and a large opening between the frontal and parietal bones that suggest ontogenetic modifications. The adult *Cyclura carinata* has a laterally compressed midbody and longer, well developed postparietal processes (Bochaton et al. 2016). Additionally, the adult specimen possesses a tall dorsal shelf and foramina across the dorsal surface that are not present on the juvenile specimen (Fig 12A).

In the adult specimens, the heavily fused elements, such as the braincase, lacked clear suture lines between component elements and were not digitally disarticulated. Although the articular and surangular exhibited more prominent boundaries, the posterior end of the two bones appeared indistinguishably fused on the three-dimensional model and showed unclear divisions

on the CT scans slices. As such, a small section of the posterior boundaries of the articular and surangular required approximation using the individual slices.

An expanded dataset of both CT data and skeletal specimens is essential for more extensive comparative analyses of intraspecific variation in cranial anatomy with *Cyclura carinata*, and interspecific variation between species of *Cyclura*. Only a few specimens were examined here (one juvenile, one mature individual, and one individual that may have been near maturity), and so our reports of intraspecific and ontogenetic variation are preliminary. Possible ontogenetic differences, such as a medial gap between diverging nasals or absent foramina, were only observed on one juvenile *Cyclura carinata* specimen (UMMZ 117401) and are difficult to confirm without more juvenile specimens. Both *Cyclura cornuta* specimens bear a well-developed, midline crest on the parietal that the *Cyclura carinata* specimens lack. A larger sampling will facilitate a deeper examination of any observed differences between the specimen skulls, allowing for a greater understanding of possible intraspecific or interspecific variation and a more consistent comparison of cranial morphology.

Identification of fossils will be an important application of our study and future studies examining the cranial osteology of species of *Cyclura*, all of which are threatened with extinction (Buckley et al. 2016; IUCN 2023). Documenting the osteological variation of extant *Cyclura* is key for identifying fossils based on morphology, and accurate fossil identifications permit a greater understanding of evolutionary and biogeographic history (Bell et al. 2010; Parham et al. 2012). Accurate identifications of fossil *Cyclura* may allow a better understanding of *Cyclura* speciation and past interactions with humans, such as how hunting by humans may have affected *Cyclura* distributions during the Holocene (Woodley 1980). Broadly, an understanding of the biology of *Cyclura*, including osteology and past distributions that can be inferred from the fossil record, will help to inform future conservation measures for this singular group of lizards.

Data

All CT data were downloaded from or are now deposited in Morphosource.org. The CT dataset for the whole body of UMMZ 117401 (Media 000070945) was acquired from https://www.morphosource.org/concern/parent/000S21327/media/000070945 The CT dataset for the head of UF 32820 (Media 000059620) was acquired from https://www.morphosource.org/concern/media/000059620. The CT dataset for MVZ 81381 was collected for this study and is now deposited at https://www.morphosource.org/XXX

Acknowledgements

We thank Jack Tseng (UC Berkeley) for scanning MVZ 81381 and the Museum of Vertebrate Zoology for loaning the specimen and other logistical support. We are grateful to David Ledesma for reviewing an earlier version of the manuscript.

References

References

1045 Avery DF. 1970. Evolution of the iguanine lizards (Sauria, Iguanidae) as determined by
1046 osteological and myological characters. Brigham Young University PhD Dissertation 7618.
1047 https://scholarsarchive.byu.edu/etd/7618
1048
1049 Avery DF, Tanner WW. 1971. Evolution of the iguanine lizards (Sauria, Iguanidae) as
1050 determined by osteological and myological characters. Brigham Young University Science
1051 Bulletin, Biological Series. vi+79 pp.
1052
1053 Bell CJ, Mead JI. 2014. Not enough skeletons in the closet: Collections-based anatomical
1054 research in an age of conservation conscience. *The Anatomical Record* 297(3):344–348.
1055 https://doi.org/10.1002/ar.22852
1056
1057 Bell CJ, Gauthier JA, Bever GS. 2010. Covert biases, circularity, and apomorphies: A critical
1058 look at the North American Quaternary Herpetofaunal Stability Hypothesis. *Quaternary*
1059 *International* 217(1–2):30–36. https://doi.org/10.1016/j.quaint.2009.08.009
1060
1061 Bochaton C, Grouard S, Breuil M, Ineich I, Tresset A, Bailon S. 201). Osteological
1062 differentiation of the *Iguana* Laurenti, 1768 (Squamata: Iguanidae) species: *Iguana iguana*
1063 (Linnaeus, 1758) and *Iguana delicatissima* Laurenti, 1768, with some comments on their
1064 hybrids. *Journal of Herpetology* 50(2):295–305. https://doi.org/10.1670/14-170
1065
1066 Buckley LJ, de Queiroz K, Grant TD, Hollingsworth BD, Iverson JB, Pasachnik SA, Stephen
1067 CL. 2016. A checklist of the iguanas of the world (Iguanidae; Iguaninae). In Iguanas:
1068 Biology, Systematics, and Conservation: Vol. (Monograph 6: pp. 4–46).
1069 http://hdl.handle.net/20.500.12634/339
1070
1071 Criley B. 1968. The Cranial Osteology of Gerrhonotiform Lizards. *American Midland Naturalist*
1072 80(1):199–219.
1073
1074 de Queiroz, Kevin. 1987. Phylogenetic systematics of iguanine lizards: A comparative
1075 osteological study. *University of California Press* 118:1–288.
1076
1077 Etheridge R, and de Queiroz K. 1988. A phylogeny of the Iguanidae. In: *Phylogenetic*
1078 *relationships of the lizard families — Essays Commemorating Charles L. Camp* (Estes R
1079 and Pregill G, editors). Stanford University Press, 283–367.
1080
1081 Evans S. 2008. The skull of lizards and tuatara. In: Gans C, Gaunt AS, Adler K, eds. Biology of
1082 the Reptilia, Volume 20, Morphology H. The Skull of Lepidosauria. New York: Society for
1083 the Study of Amphibians and Reptiles.
1084
1085 Fedorov A, Beichel R, Kalpathy-Cramer J, Finet J, Fillion-Robin J-C, Pujol S, Bauer C, Jennings
1086 D, Fennessy F, Sonka M, Buatti J, Aylward S, Miller JV, Pieper S, Kikinis R. 2012. 3D
1087 Slicer as an image computing platform for the Quantitative Imaging Network. *Magnetic*
1088 *Resonance Imaging* 30(9):1323–1341. https://doi.org/10.1016/j.mri.2012.05.001
1089

1090 Gerber GP, Colosimo G, Grant TD. 2020. *Cyclura carinata*. The IUCN Red List of Threatened
1091 Species 2020: e.T6026A3097754. https://dx.doi.org/10.2305/IUCN.UK.2020-
1092 2.RLTS.T6026A3097754.en
1093
1094 González Rodríguez E, Encinoso Quintana M, Morales Bordon D, Garcés JG, Artiles Nuez H, &
1095 Jaber JR. 2023. Anatomical description of rhinoceros iguana (*Cyclura cornuta cornuta*)
1096 head by computed tomography, magnetic resonance imaging and gross-sections. *Animals*
1097 13(6):955. https://doi.org/10.3390/ani13060955
1098
1099 Gauthier JA, Kearney M, Maisano JA, Rieppel O, Behlke ADB. 2012. Assembling the squamate
1100 tree of life: Perspectives from the phenotype and the fossil record. Bulle*tin of the Peabody*
1101 *Museum of Natural History* 53(1):3–308. https://doi.org/10.3374/014.053.0101
1102
1103 Hernández-Jaimes C, Jerez A, Ramírez-Pinilla MP. 2012. Embryonic development of the skull
1104 of the Andean lizard *Ptychoglossus bicolor* (Squamata, Gymnophthalmidae). *Journal of*
1105 *Anatomy* 221(4):285-302. https://doi.org/10.1111/j.1469-7580.2012.01549.x
1106
1107 Iverson J. 1979. Behavior and ecology of the rock iguana *Cyclura carinata*. *Bulletin of the*
1108 *Florida Museum of Natural History* 24(3):175–358.
1109
1110 IUCN. 2023. The IUCN Red List of Threatened Species. Version 2023-1.
1111 https://www.iucnredlist.org. Accessed on 4 December, 2023.
1112
1113 Keogh JS, Edwards DL, Fisher RN, Harlow PS. 2008. Molecular and morphological analysis of
1114 the critically endangered Fijian iguanas reveals cryptic diversity and a complex
1115 biogeographic history. P*hilosophical Transactions of the Royal Society B: Biological*
1116 *Sciences* 363(1508):3413–3426. https://doi.org/10.1098/rstb.2008.0120
1117
1118 LeBlanc ARH, Paparella I, Lamoureux DO, Doschak MR, Caldwell MW. 2021. Tooth
1119 attachment and pleurodont implantation in lizards: Histology, development, and evolution.
1120 *Journal of Anatomy* 238(5):1156-1178. https://doi.org/10.1111/joa.13371
1121
1122 Ledesma DT, Scarpetta SG, Bell CJ. 2021. Variation in the skulls of *Elgaria* and *Gerrhonotus*
1123 (Anguidae, Gerrhonotinae) and implications for phylogenetics and fossil identification.
1124 *PeerJ* 9:e11602. https://doi.org/10.7717/peerj.11602
1125
1126 Ledesma DT, Scarpetta SG, Jacisin III JJ, Meza A, Kemp ME. 2023. Identification of Late
1127 Pleistocene and Holocene fossil lizards from Hall's Cave and a primer on morphological
1128 variation in North American lizard skulls. *bioRxiv*, 2023-07.
1129
1130 Maisano JA. 2002. Postnatal skeletal ontogeny in *Callisaurus draconoides* and *Uta stansburiana*
1131 (Iguania: Phrynosomatidae). *Journal of Morphology* 251(2):114–139.
1132 https://doi.org/10.1002/jmor.1078
1133
1134 Montanucci RR. 1968. Comparative dentition in four iguanid lizards. *Herpetologica* 24(4):305-
1135 315

Norell MA, de Queiroz K. 1991. The earliest iguanine lizard (Reptilia: Squamata) and its bearing on iguanine phylogeny." *The American Museum of Natural History* 2997(16):1–17.

Oelrich TM. 1956. The anatomy of the head of *Ctenosaura pectinata* (Iguanidae). *Miscellaneous Publications Museum of Zoology*, *University of Michigan* 94:1–122.

Paparella I, Caldwell MW. 2022. Cranial anatomy of the Galápagos marine iguana *Amblyrhynchus cristatus* (Squamata: Iguanidae). *The Anatomical Record* 305(7):1739–86, https://doi.org/10.1002/ar.24797.

Parham JF, Donoghue PCJ, Bell CJ, Calway TD, Head JJ, Holroyd PA, Inoue JG, Irmis RB, Joyce WG, Ksepka DT, Patané JSL, Smith ND, Tarver JE, Van Tuinen M, Yang Z, Angielczyk KD, Greenwood JM, Hipsley CA, Jacobs L, Makovicky PJ, Müller J, Smith KT, Theodor JM, Warnock RCM, Benton MJ. 2012. Best practices for justifying fossil calibrations. *Systematic Biology* 61(2):346–359. https://doi.org/10.1093/sysbio/syr107

Porter WR, Witmer LM. 2015. Vascular patterns in iguanas and other squamates: Blood vessels and sites of thermal exchange. *PLOS ONE,*10(10):e0139215. https://doi.org/10.1371/journal.pone.0139215

Powell R. 2000. *Cyclura onchiopsis* Cope Navass Island Rhinoceros Iguana. *Catalogue of American Amphibians and Reptiles*, 710.1–710.3.

Rolfe S, Pieper S, Porto A, Diamond K, Winchester J, Shan S, Kirveslahti H, Boyer D, Summers A, Maga AM. 2021. SlicerMorph: An open and extensible platform to retrieve, visualize and analyse 3D morphology. *Methods in Ecology and Evolution* 12(10):1816–1825. https://doi.org/10.1111/2041-210X.13669

Simões TR, Caldwell MW, Tałanda M, Bernardi M, Palci A, Vernygora O, Bernardini F, Mancini L, Nydam RL. 2018. The origin of squamates revealed by a Middle Triassic lizard from the Italian Alps. *Nature* 557(7707):706–709. https://doi.org/10.1038/s41586-018-0093-3

Smith KT. 2009. Eocene lizards of the clade *Geiseltaliellus* from Messel and Geiseltal, Germany, and the early radiation of Iguanidae (Reptilia: Squamata). *Bulletin of the Peabody Museum of Natural History* 50(2):219–306. https://doi.org/10.3374/014.050.0201

Tarazona OA, Ramírez-Pinilla MP. 2008. The unusual orbitosphenoid of the snakelike lizard *Bachia bicolor*. Journal of Anatomy; 213:130-139. https://doi.org/10.1111/j.1469-7580.2008.00939.x

Villa, Andrea, Daza JD, Bauer AM, Delfino M. 2018. Comparative Cranial Osteology of European Gekkotans (Reptilia, Squamata). *Zoological Journal of the Linnean Society*; 184(3):1–39. https://doi.org/10.1093/zoolinnean/zlx104

Watanabe A, Fabre A-C, Felice RN, Maisano JA, Müller J, Herrel A, Goswami A. 2019. Ecomorphological diversification in squamates from conserved pattern of cranial integration. *Proceedings of the National Academy of Sciences of the United States of America* 116(29):14688–14697. https://doi.org/10.1073/pnas.1820967116

Winchell KM, Campbell-Staton SC, Losos JB, Revell LJ, Verrelli BC, Geneva AJ. 2023. Genome-wide parallelism underlies contemporary adaptation in urban lizards. *Proceedings of the National Academy of Sciences of the United States of America* 120(3):e2216789120. https://doi.org/10.1073/pnas.2216789120

Woodley JD. 1980. Survival of the Jamaican iguana, *Cyclura collei*. *Journal of Herpetology* 14(1):45–49. https://doi.org/10.2307/1563874

Table 1(on next page)

Table 1. Raw CT data sources and parameter settings for Cyclura carinata.

Raw CT data sources and parameter settings for Cyclura carinata.

1 **Table 1. Raw CT data sources and parameter settings for *Cyclura carinata*.**
2

Specimen	Date and Locality	Scanner	Facility	CT slices in XY plane	X-ray settings	Voxel Size (mm)
UF Herp 32820	1974, Turks and Caicos, Pine Cay	General electric phoenix c|tome|x m240 scanner	UF Nanoscale Research Facility	6013	100 kV, 0.25 mA	0.111482
UMMZ 117401	1953, Turks and Caicos, Long Cay	Nikon Metrology XT H 225 ST	UMMZ Research Museums Center	1908	85 kV, 0.2 mA	0.076494
MVZ 81381	1964, Turks and Caicos, Turks Island	General Electric phoenix nanotom m 180	UCB FAVE Lab	3000	70 kV, 0.220 mA	0.036739

3

Table 2(on next page)

Table 2. Anatomical Abbreviations

Anatomical Abbreviations

1 **Table 2. Anatomical Abbreviations.**

Abbreviation	Anatomical Structure
1cb	First ceratobranchial
1eb	First epibranchial
2cb	Second ceratobranchial
a.ar	Anterior ampullar recess
a.ia.f	Anterior inferior alveolar foramen
a.m.fo	Anterior mylohyoid foramen (fossa)?
a.Mk.fs	Anterior opening of Meckelian fossa
a.San.f	Anterior surangular foramen
a.vc	Anterior vidian canal opening
ab.f	Abducens foramen
ad.cr	Adductor crest
ad.fs	Adductor fossa
aip	Anterior inferior process
al.pr	Anterolateral process
al.Px.pr	Anterolateral premaxillary process
alv.p	Alveolar plate
am.pr	Anteromedial process
am.pr	Anteromedial process
am.Px.pr	Anteromedial premaxillary process
An	angular
an.pr	Angular process
Art	Articular
bh	basihyal
Bo	Basioccipital

Bo.co	Basioccipital condyle
Bt.pr	Basipterygoid process
c.co	Central column
cch	conch
ce.co	Cephalic condyle
Co	Coronoid
co.am.pr	Anteromedial process of coronoid
co.ft	Coronoid facet
co.pm.pr	Posteromedial process of coronoid
cr	crest
cr.cr	Crista cranii
cr.if	Crista interfenestralis
cr.Pro	Crista prootica
cr.s	Crista sellaris
cr.tb	Crista tuberalis
crt	Crista transversalis (?)
D	Dentary
d.s	Dorsum sella
Ec	Ectopterygoid
eh	Epihyoid
et.f	Ethmoidal foramen
f.12	Foramina for hypoglossal nerve
f.7	Foramen for facial nerve
f.8	Foramen for vestibulocochlear nerve
f.co	Fossa columella
f.mg	Foramen magnum

f.o	Fenestra ovalis
fe	Free epibranchial
Fr	Frontal
Fr.n.ft	Nasal facet of frontal
hc	Hyoid cornu
Hy	Hyoid
i.o.f	Infraorbital foramen
i.pro	Incisura prootica
icf	Internal carotid foramen
J	Jugal
J.p.pr	Posterior process of jugal
L	lacrimal
L.f	Lacrimal foramen
L.pv.pr	Lacrinal posteroventral process
lhv.n	Notch for the lateral head vein
lrst	Lateral aperature for the recessus scali tympani
ma.co	Mandibular condyle
ma.co.ft	Mandibular condyle facet
ma.sy	Mandibular symphysis
mrst	Medial aperture for the recessus scali tympani
Mx	Maxilla
Mx.f.pr	Maxillary facial process
Mx.j.pr	Jugal process of maxilla
Mx.pr	Maxillary process
Mx.sh	Maxillary shelf

N	Nasal
N.al.pr	Anterolateral process of nasal
N.am.pr	Anteromedial process of nasal
n.f	Nutrient foramen
N.fr.pr	Frontal process of nasal
nu.fo	Nucal fossa
o.pr	Orbital process
Ot	Otooccipital
P	Parietal
P.a.pr	Parietal anterior process
P.f	Parietal foramen
P.fo	Parietal fossa
p.m.f	
p.San.f	Posterior surangular foramen
p.ta	Parietal table
p.vc	Posterior opening of vidian canal
pa.pr	Palatal process
Pa.pr	Palatine process
Pfr	Postfrontal
Pfr.ft	Postfrontal facet
pit.fo	Pituitary fossa
pl	Processus lingualis
Po	postorbital
Po.pr	Postorbital process
poc.pr	Paraoccipital process
pp.pr	Postparietal (supratemporal) process

pr.as	Processus ascendens
Prf	Prefrontal
Prf.am.pr	Anteromedial process of prefrontal
Prf.pv.pr	Posteroventral process of prefrontal
Pro	Prootic
Pro.a.pr	Anterior process of prootic
psp.pr	Parasphenoid process
Pt.lm	Pterygoid lamina
Pt.t	Pterygoid teeth
Px	premaxilla
Px.a.f	Premaxilla anterior foramen
Px.n.pr	Premaxillary nasal process
Px.pr	Premaxillary process
Q	Quadrate
Q.pr	Quadrate process
r.v.j	Recessus vena jugularis
ra.pr	Retroarticular process
s.t	Sella turcica
sac	Superior alveolar canal
San	Surangular
san.pr	Surangular process
sd.sh	Subdentary shelf
So	Supraoccipital
sof	Suborbital fenestra
Sp	Sphenoid
Sp	Sphenoid

Sp.a.pr	Anterior process of sphenoid
Sq	squamosal
St	supratemporal
st.pr	Supratrigeminal process
Stp	Stapes
Sx.a.pr	Septomaxilla anterior process
Sx.d.pr	Septomaxilla dorsal process
Sx.v.pr	Septomaxilla ventral process
Ta	Trachea
t.cr	Tympanic crest
tr	trabecula
v.ch	Vomer choana
v.f	Vagus foramen
v.pr	Ventral process
vl.ft	Ventrolateral facet
vl.Pt.fl	Ventrolateral pterygoid flange
vm.pr	Ventromedial process
vm.Pt.fl	Ventromedial pterygoid flange
Vo.pr	Vomerine process

2
3

Figure 1

Full skull dorsal view

Dorsal view of the entire skull of Cyclura carinata UF Herp 32820. Scale bar = 10 mm.

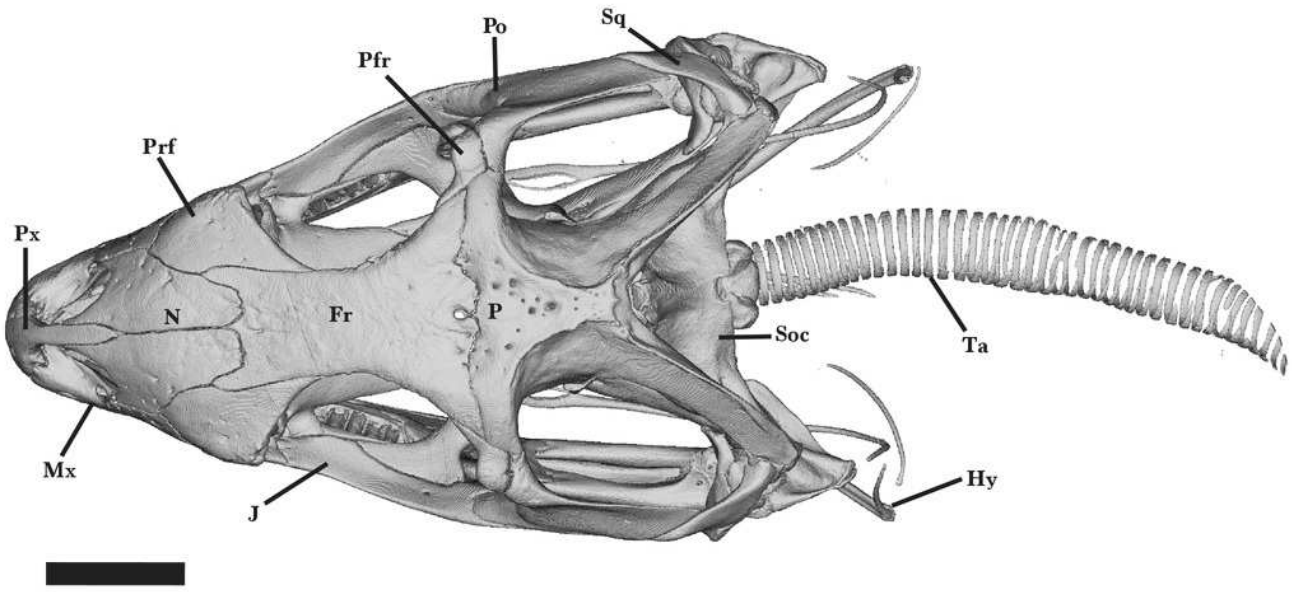

Figure 2

Reference_skull_lateral_view

Lateral view of the entire skull of Cyclura carinata UF Herp 32820. Scale bar = 10 mm.

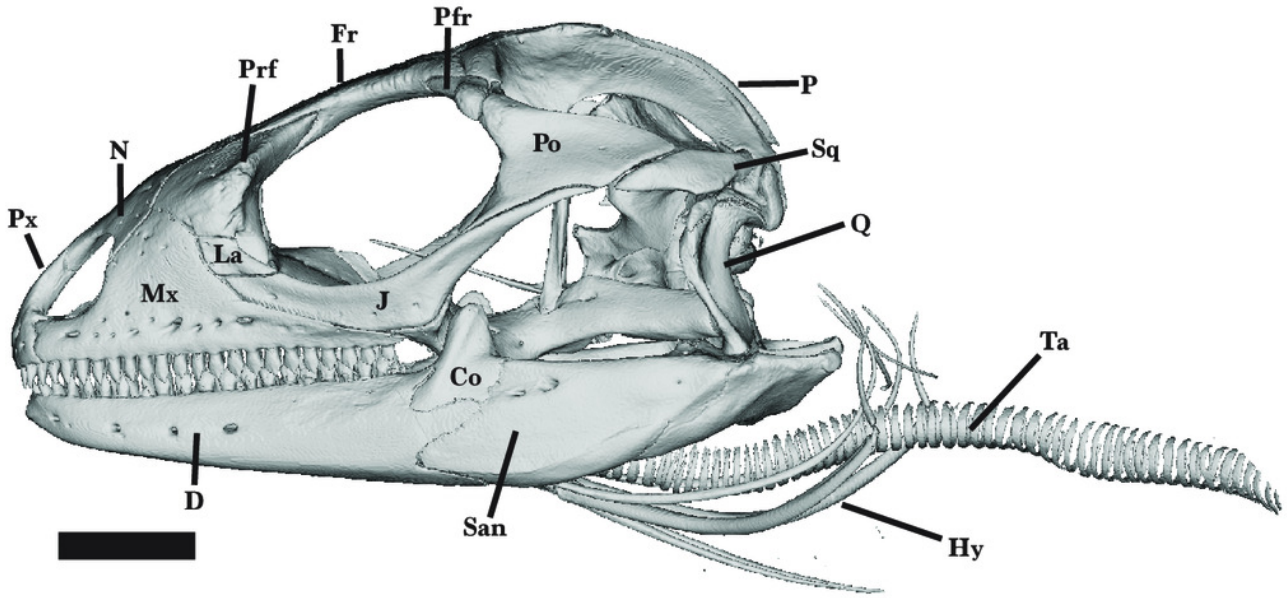

Figure 3

Full_palatal_bones

Palatal bones of Cyclura carinata UF Herp 32820. A dorsal view, B ventral view. Scale bar = 10 mm.

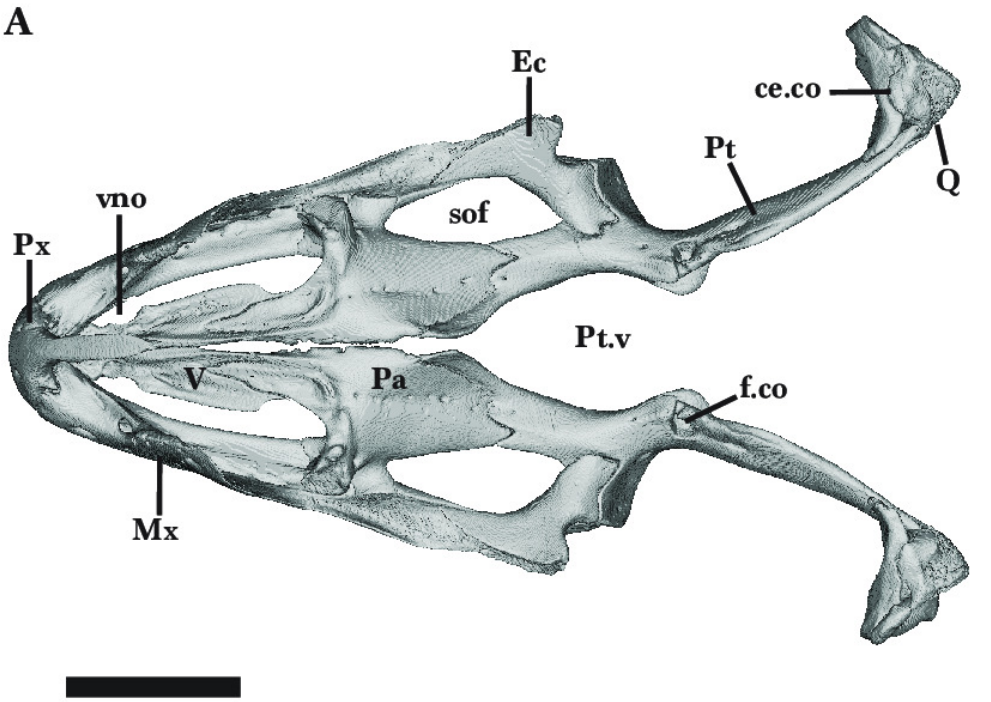
A
Ec
ce.co
Pt
Q
vno
sof
Px
Pt.v
V
Pa
f.co
Mx

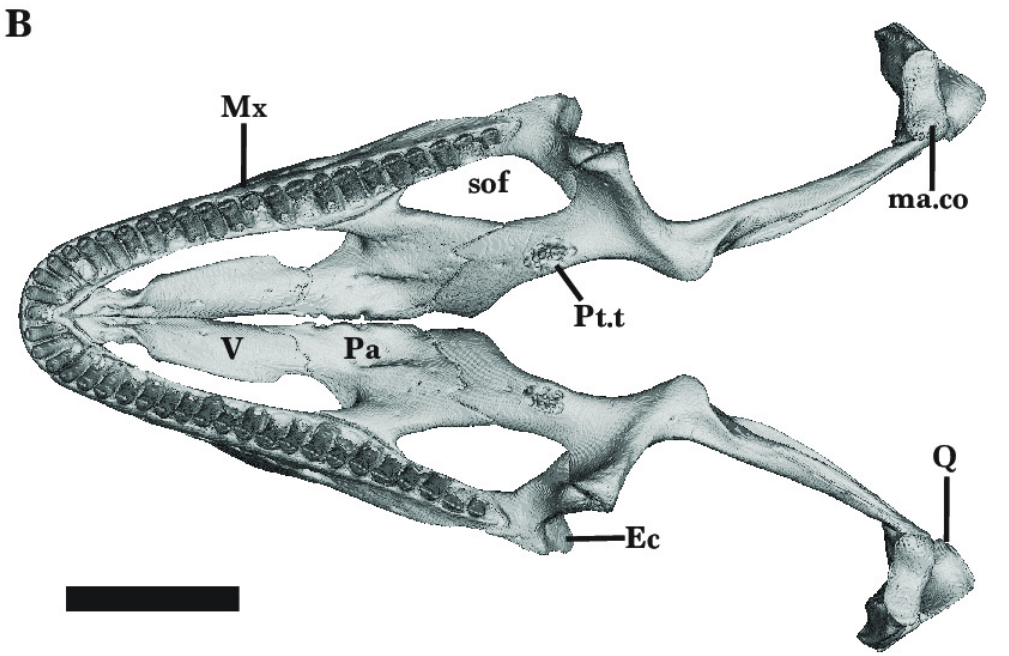
B
Mx
sof
ma.co
Pt.t
V
Pa
Q
Ec

Figure 4

Right Dentary

Right dentary of Cyclura carinata UF Herp 32820. A ventral view, B medial view, C lateral view. Scale bar = 1 mm, 10 mm for reference skull.

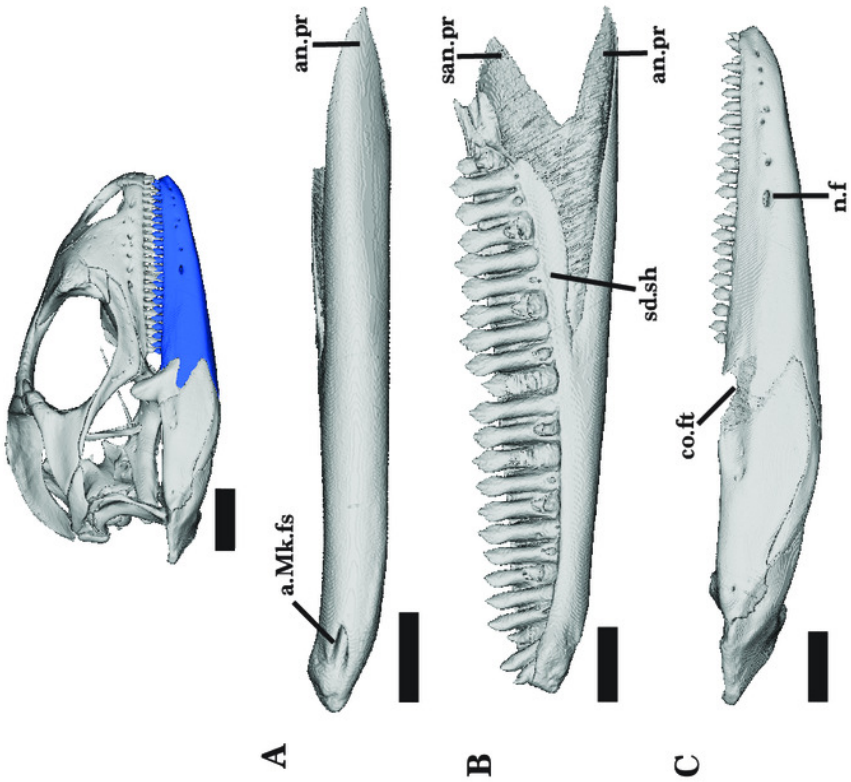

Figure 5

Left Coronoid

Left coronoid of Cyclura carinata UF Herp 32820. A lateral view, B posteromedial view. Scale bar = 5 mm, 10 mm for reference skull.

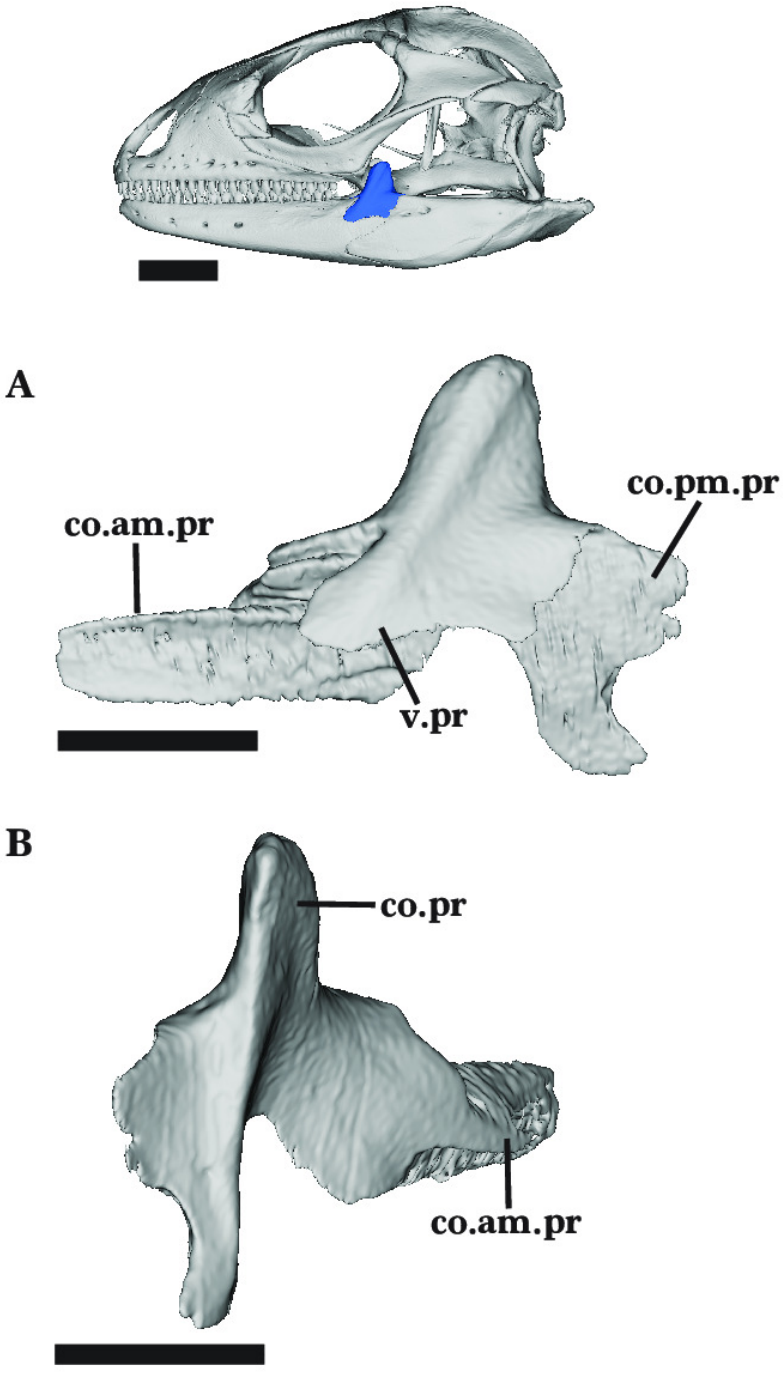
A
co.am.pr
co.pm.pr
v.pr
B
co.pr
co.am.pr

Figure 6

Right_Mandible_overview

Right mandible of Cyclura carinata UF Herp 32820. A medial view, B lateral view. Scale bar = 1 mm, 10 mm for reference skull.

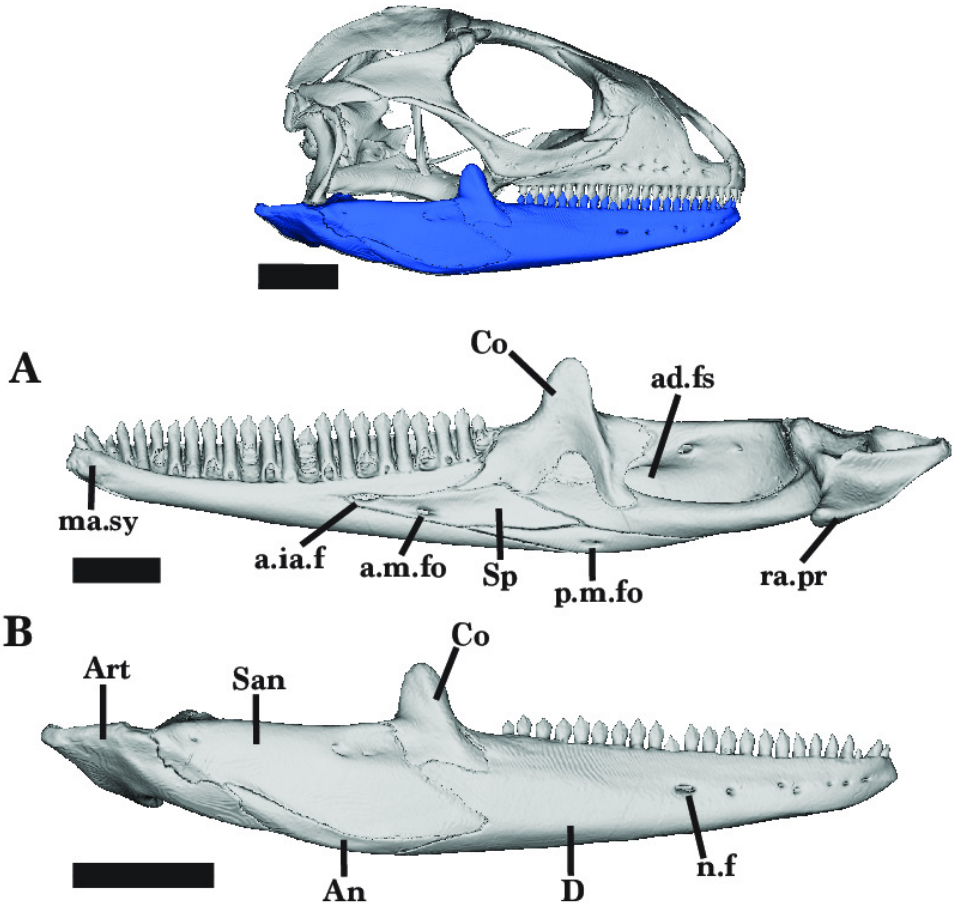
A
Co
ad.fs
ma.sy
a.ia.f
a.m.fo
Sp
p.m.fo
ra.pr
B
Co
Art
San
An
D
n.f

Figure 7

Right_Articular_Surangular

Right articular and surangular of Cyclura carinata UF Herp 32820. A lateral view, B medial view, C ventral view. Scale bar = 1 mm, 10 mm for reference skull.

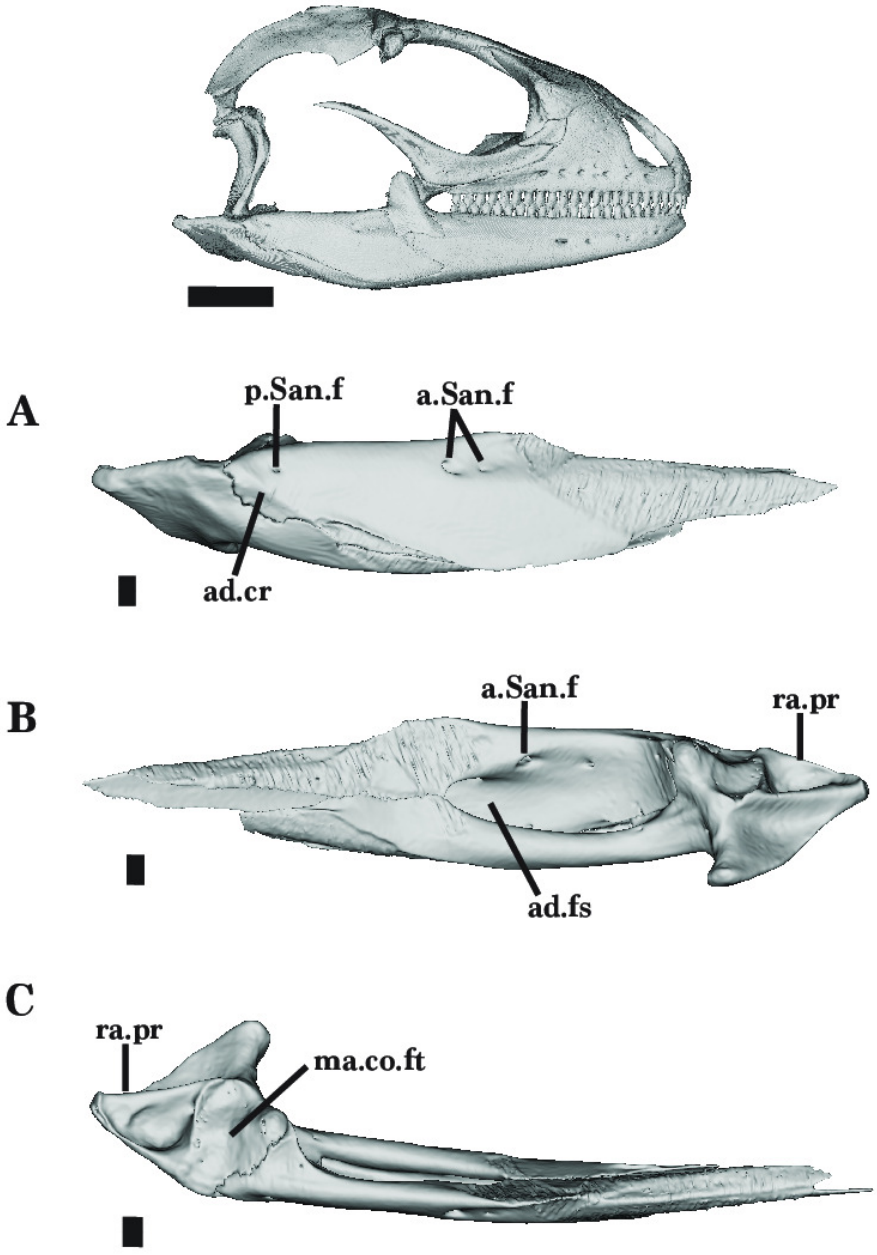
A
p.San.f
a.San.f
ad.cr
B
a.San.f
ra.pr
ad.fs
C
ra.pr
ma.co.ft

Figure 8

Premaxilla

Premaxilla of Cyclura carinata UF Herp 32820. A anterior view, B posterior view, C lateral view. Scale bar = 1 mm.

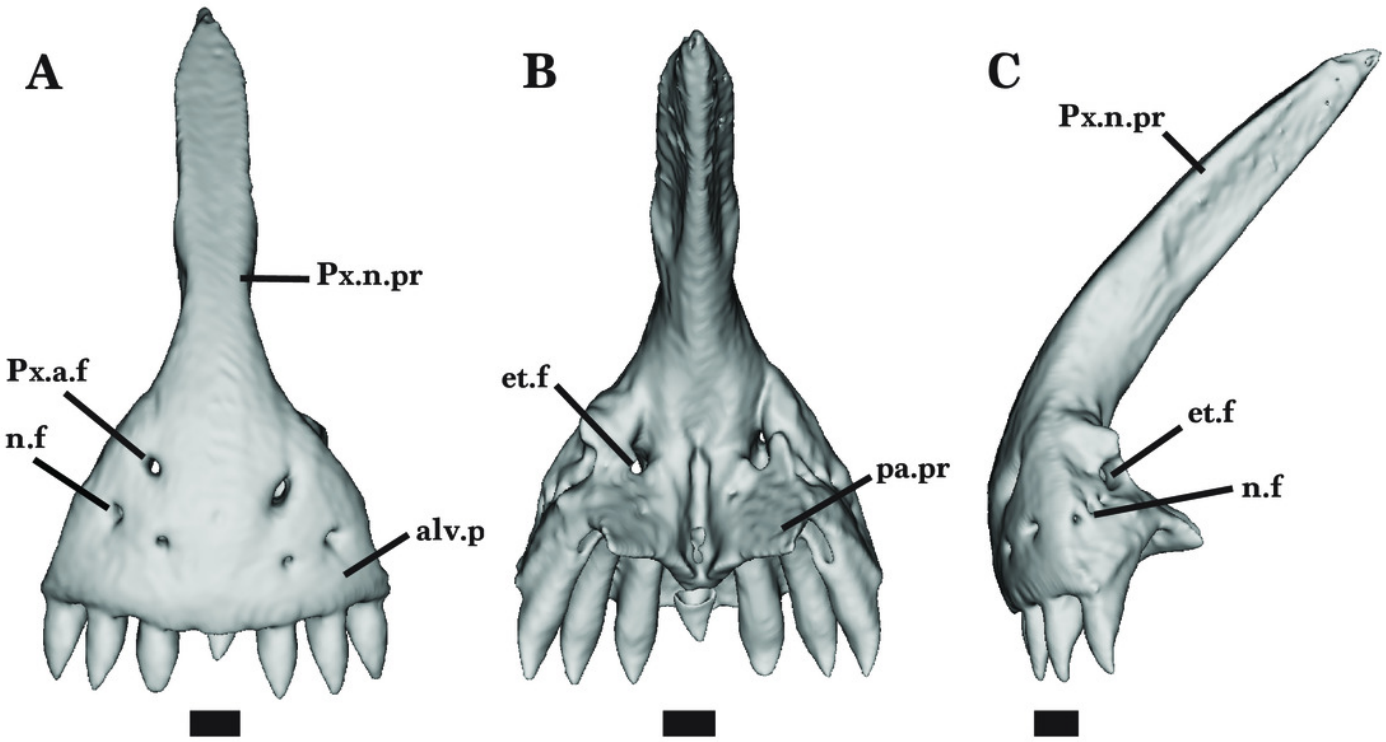

Figure 9

Left Maxilla

Left maxilla of Cyclura carinata UF Herp 32820. A lateral view, B medial view, C anterior view. Scale bar = 5 mm, 10 mm for reference skull.

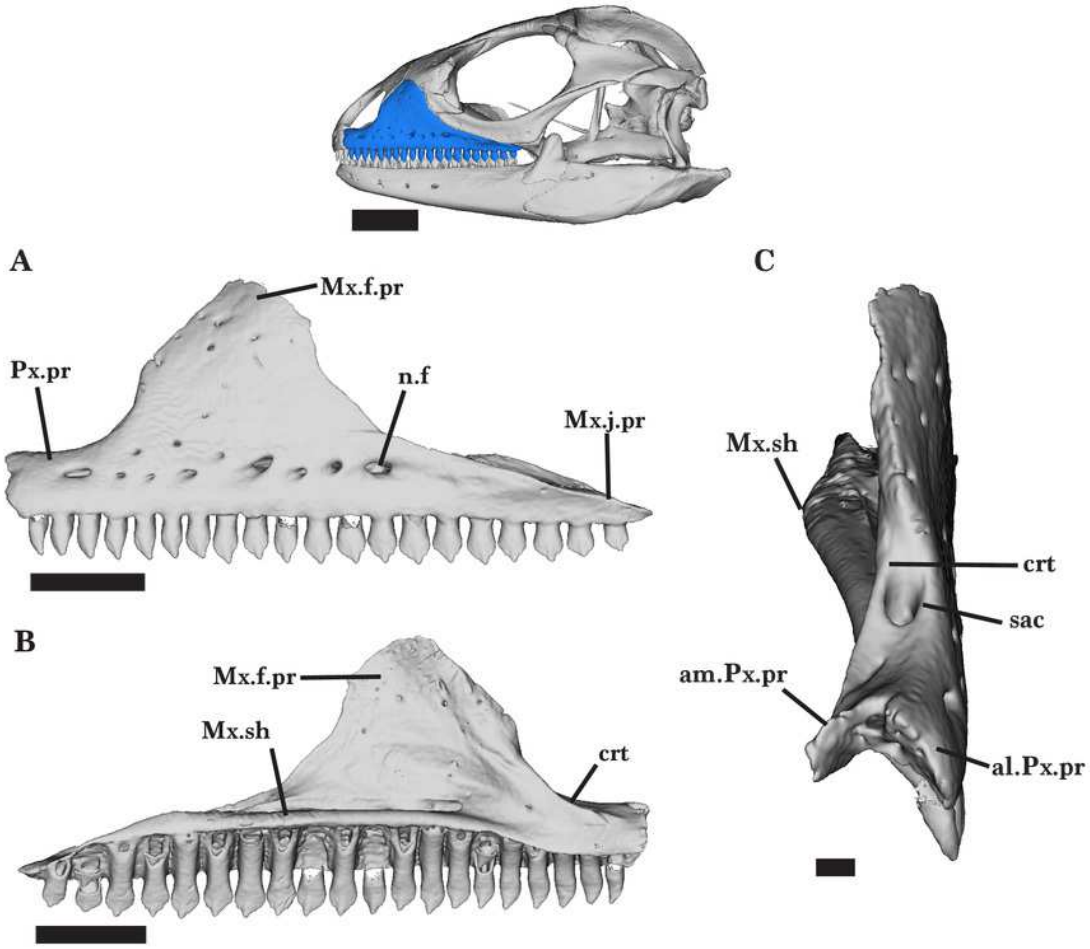

Figure 10

Nasals

Nasals of Cyclura carinata UF Herp 32820. A dorsal view, B ventral view. Scale bar = 5 mm, 10 mm for reference skull.

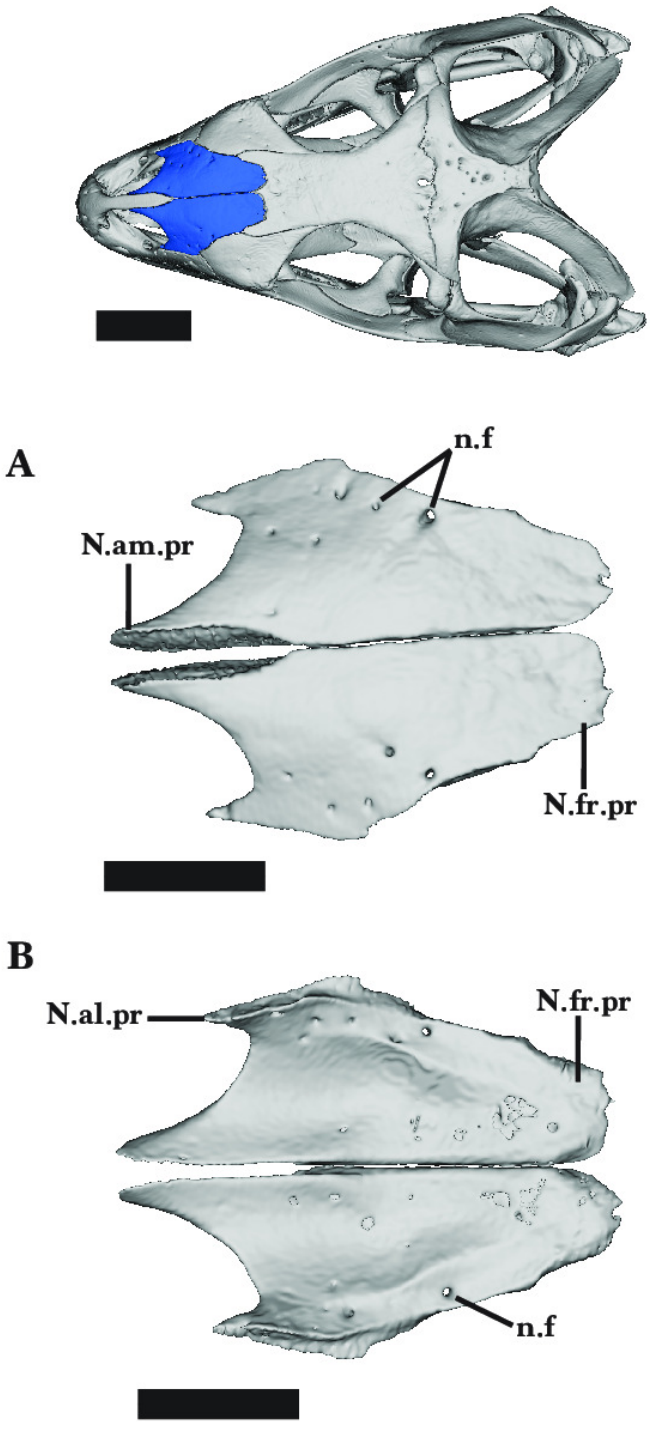
A
n.f
N.am.pr
N.fr.pr
B
N.al.pr
N.fr.pr
n.f

Figure 11

Frontal

Frontals of Cyclura carinata UF Herp 32820. A dorsal view, B ventral view. Scale bar = 1 mm, 10 mm for reference skull.

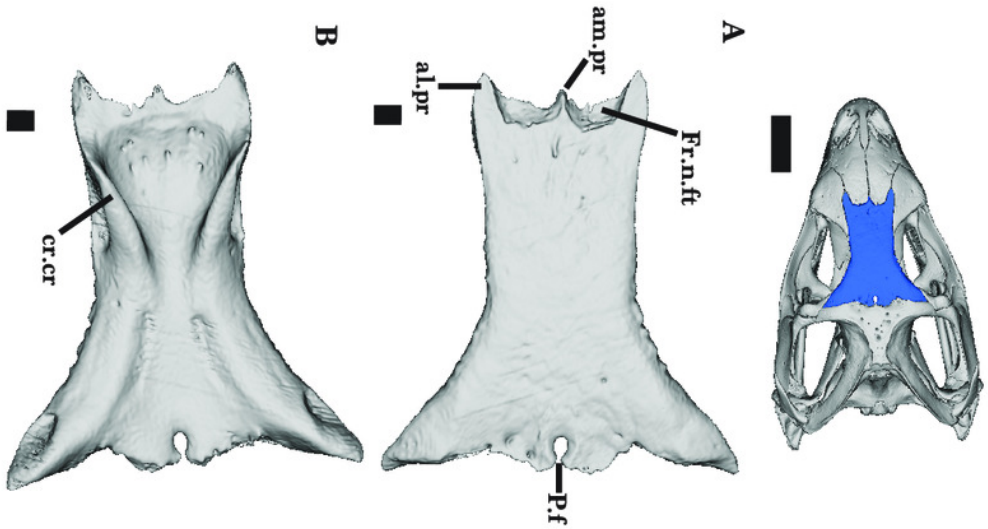

Figure 12

Frontal and Parietal

Frontal and Parietal of Cyclura carinata UF Herp 32820. A dorsal view, B ventral view. Scale bar = 10 mm.

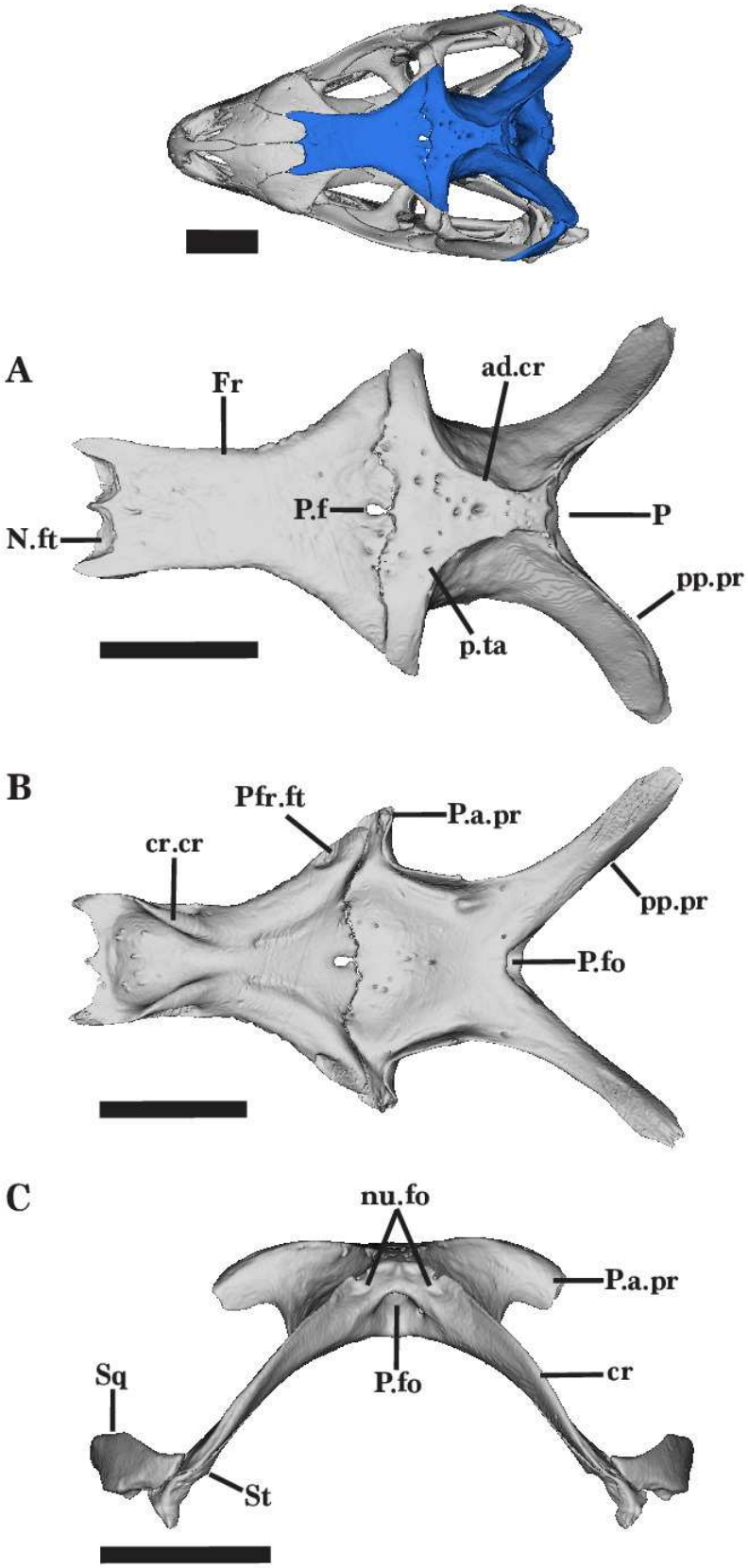
A
Fr
ad.cr
P.f
P
N.ft
pp.pr
p.ta
B
Pfr.ft
P.a.pr
cr.cr
pp.pr
P.fo
C
nu.fo
P.a.pr
Sq
P.fo
cr
St

Figure 13

Right_Prefrontal_and_Lacrimal

Lacrimal and prefrontal of Cyclura carinata UF Herp 32820. A right prefrontal and lacrimal in posterior view, B right prefrontal in lateral view, C right lacrimal in lateral view. Scale bar = 5 mm, 10 mm for reference skull.

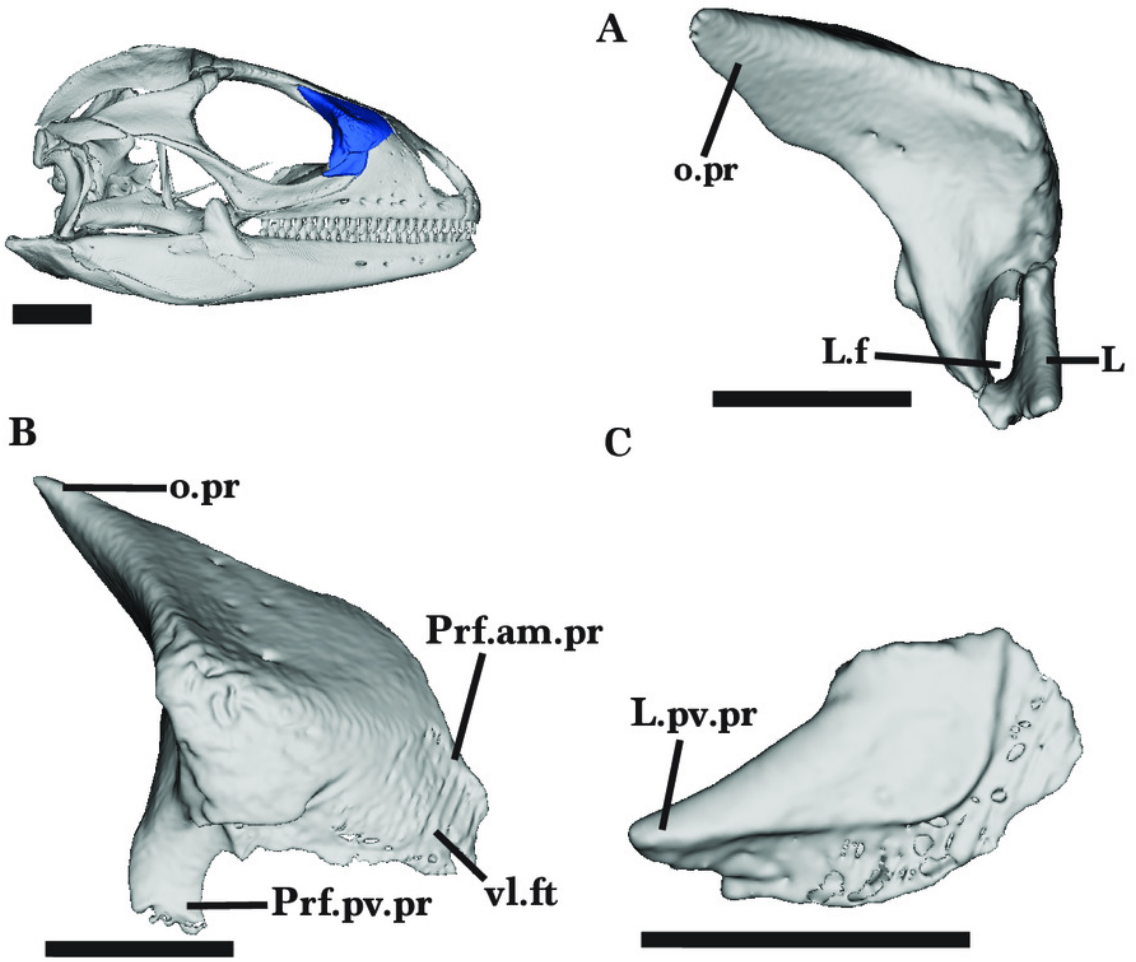
A
o.pr
L.f
L
B
o.pr
Prf.am.pr
Prf.pv.pr
vl.ft
C
L.pv.pr

Figure 14

Right_lacrimal_jugal_postorbital_ectopterygoid

Right lacrimal, jugal, ectopterygoid, and postorbital of Cyclura carinata UF Herp 32820. A lateral view, B medial view. Scale bar = 10 mm.

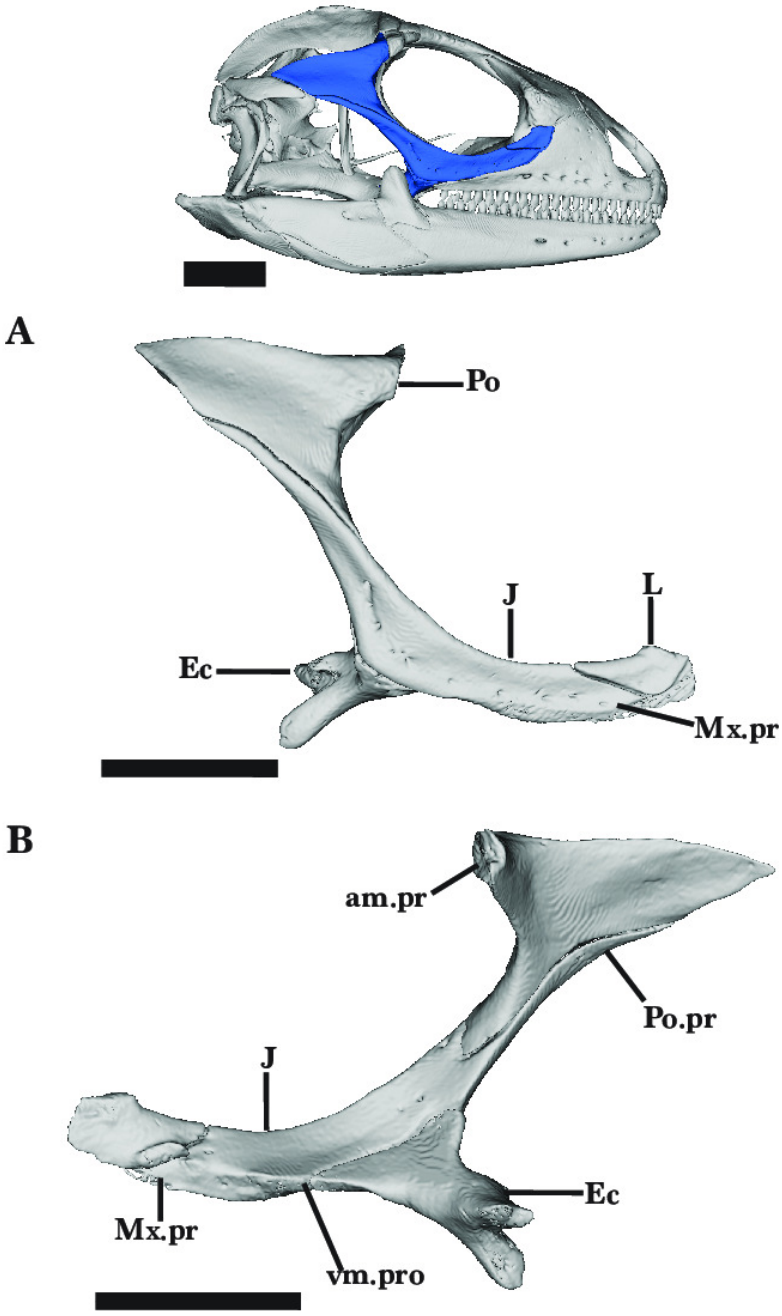
A
Po
J
L
Ec
Mx.pr
B
am.pr
Po.pr
J
Ec
Mx.pr
vm.pro

Figure 15

Right Quadrate

Right quadrate of Cyclura carinata UF Herp 32820. A anterior view, B right lateral view, C posterior view, D left lateral view. Scale bar = 1 mm, 10 mm for reference skull.

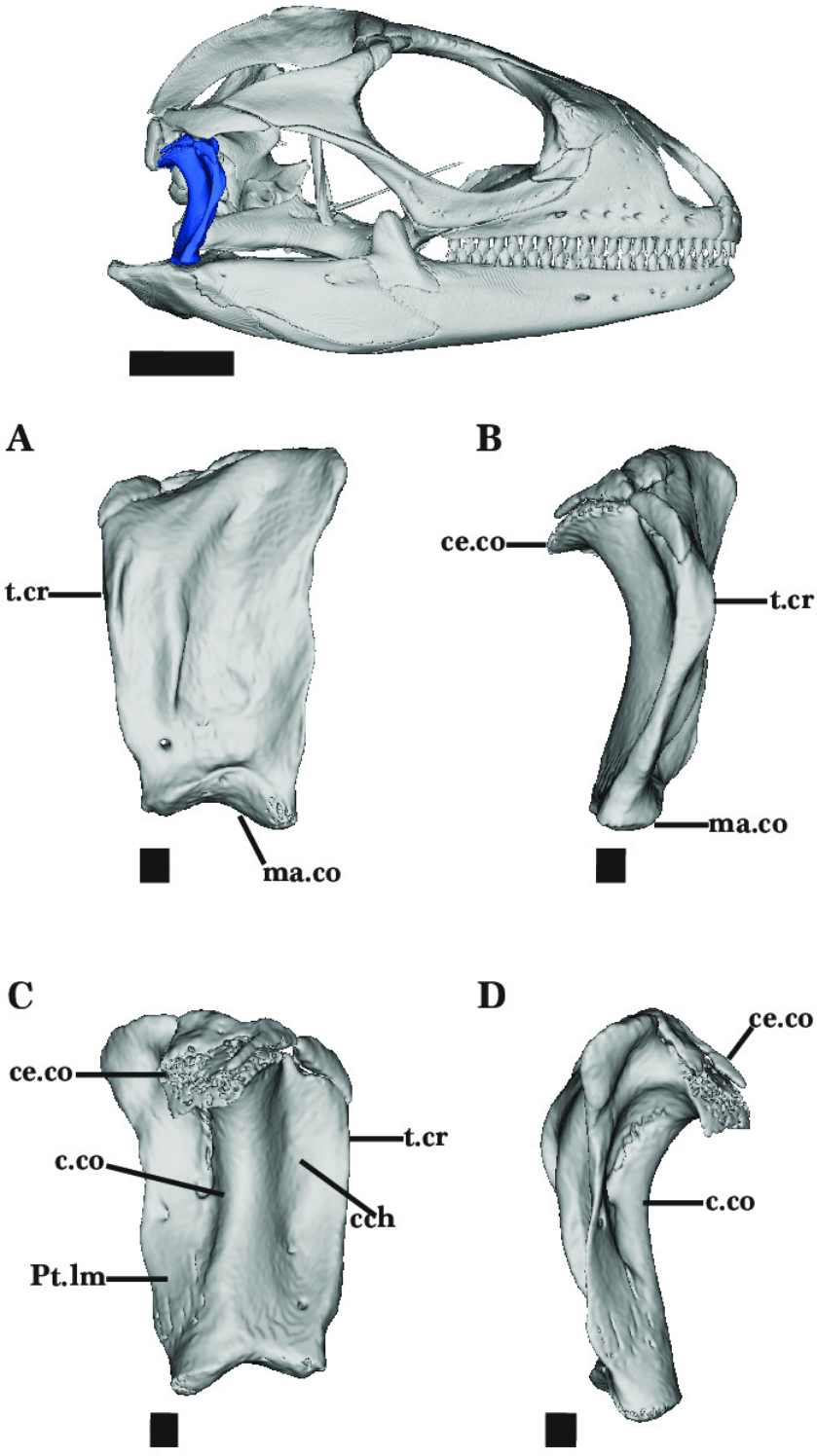
A
t.cr
ma.co
B
ce.co
t.cr
ma.co
C
ce.co
t.cr
c.co
cch
Pt.lm
D
ce.co
c.co

Figure 16

Right Palatal Bones

Right palatal bones of Cyclura carinata UF Herp 32820. A ventral view, B dorsal view. Scale bar = 10 mm.

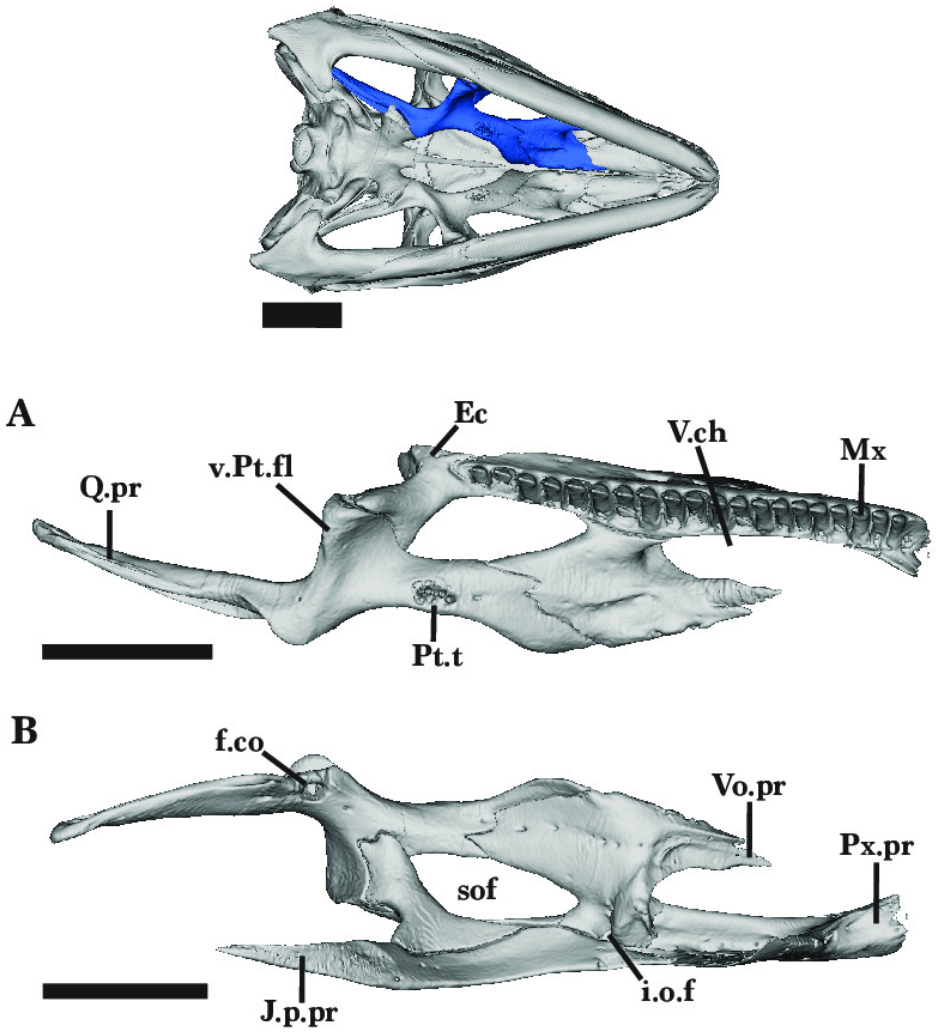
A
Ec
V.ch
Mx
v.Pt.fl
Q.pr
Pt.t
B
f.co
Vo.pr
Px.pr
sof
i.o.f
J.p.pr

Figure 17

Right Pterygoid

Right pterygoid of Cyclura carinata UF Herp 32820. A anterior view, B dorsal view. Scale bar = 10 mm.

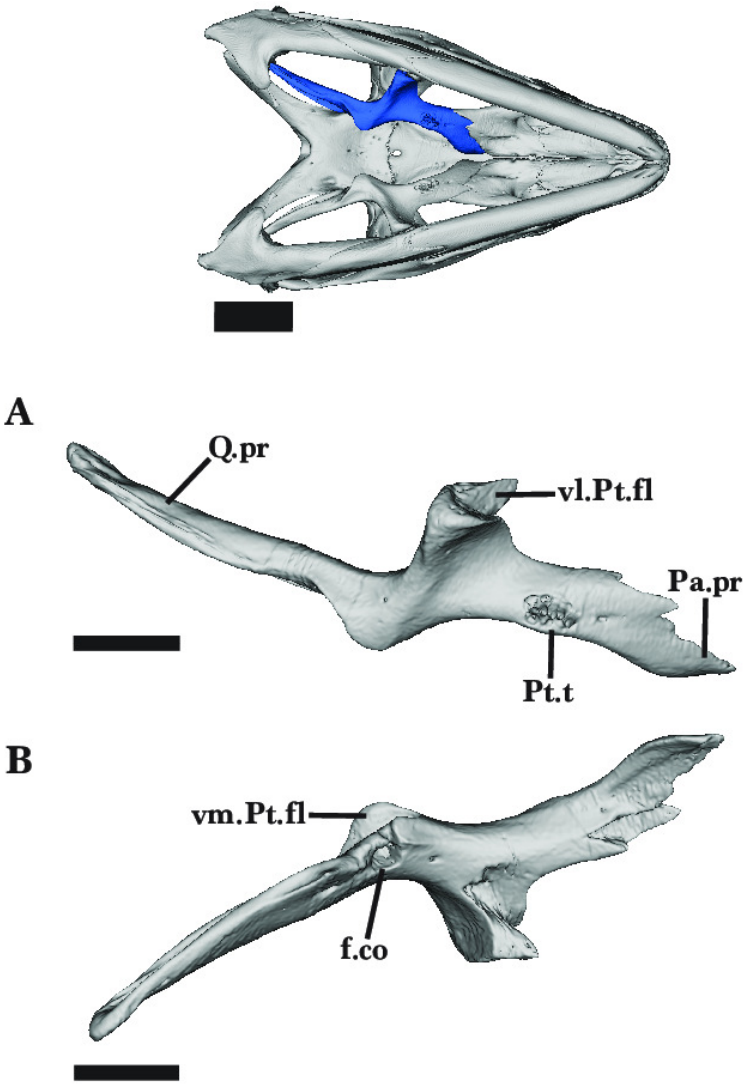
A
Q.pr
vl.Pt.fl
Pa.pr
Pt.t
B
vm.Pt.fl
f.co

Figure 18

Septomaxillae

Septomaxillae of Cyclura carinata UF Herp 32820. A anterior view, B lateral view. Scale bar = 1 mm, 10 mm for reference skull.

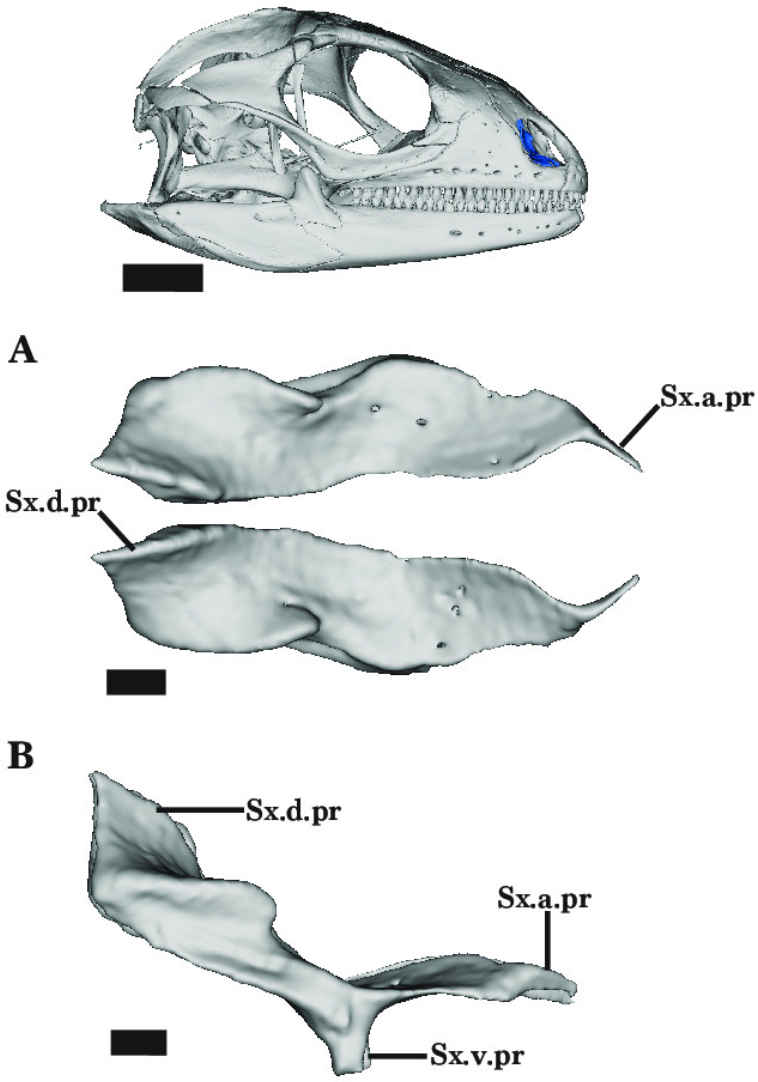
A
Sx.a.pr
Sx.d.pr
B
Sx.d.pr
Sx.a.pr
Sx.v.pr

Figure 19

General Braincase 1

General braincase of Cyclura carinata UF Herp 32820. A dorsal view, B posterior view. Scale bar = 10 mm.

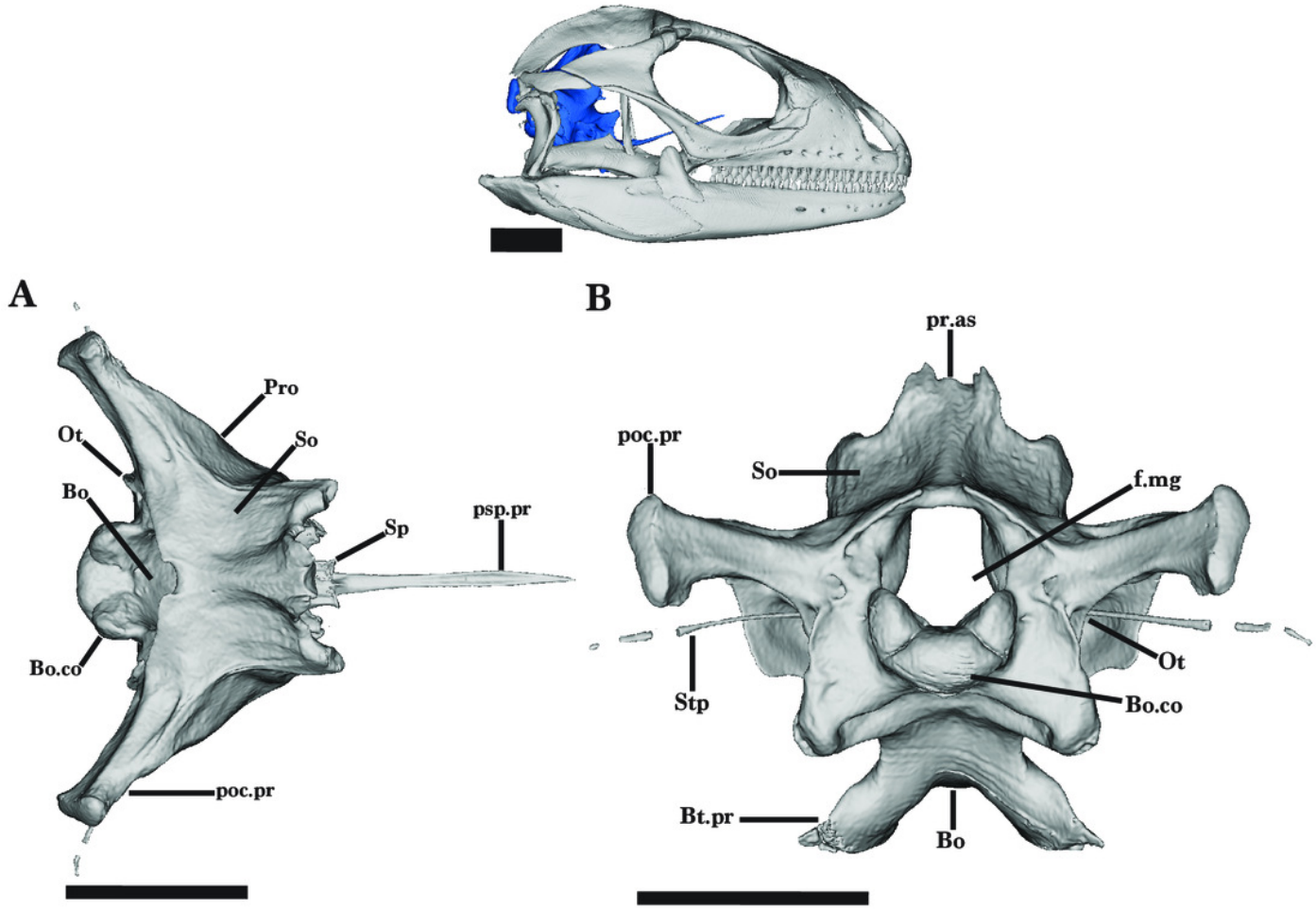
A
Pro
Ot
So
Bo
Sp
psp.pr
Bo.co
poc.pr
B
pr.as
poc.pr
So
f.mg
Ot
Stp
Bo.co
Bt.pr
Bo

Figure 20

General Braincase 2

General braincase of Cyclura carinata UF Herp 32820. A anterior view, B anterolateral view. Scale bar = 10 mm.

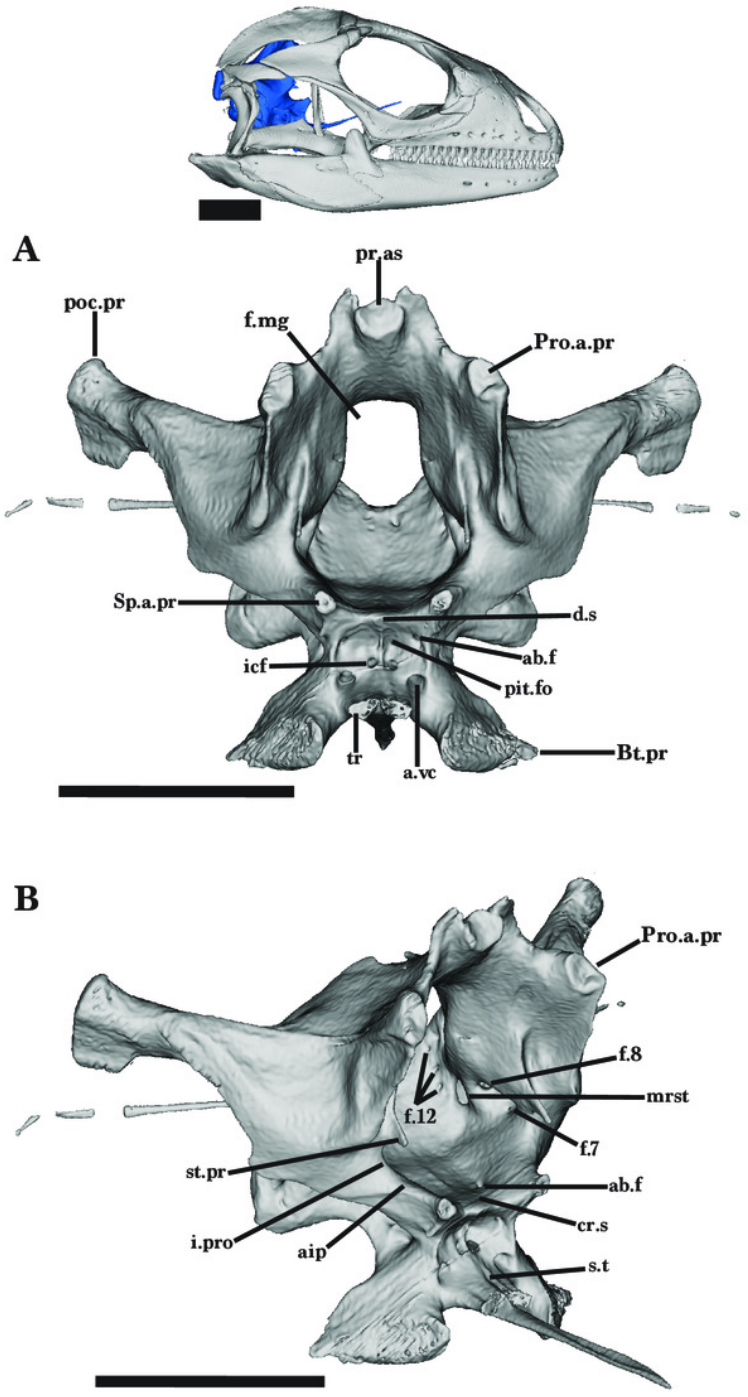
A
pr.as
poc.pr
f.mg
Pro.a.pr
Sp.a.pr
d.s
ab.f
icf
pit.fo
tr
a.vc
Bt.pr
B
Pro.a.pr
f.8
mrst
f.12
f.7
st.pr
ab.f
cr.s
i.pro
aip
s.t

Figure 21

General Braincase 3

General braincase of Cyclura carinata UF Herp 32820. A lateral view, B posterolateral view. Scale bar = 10 mm.

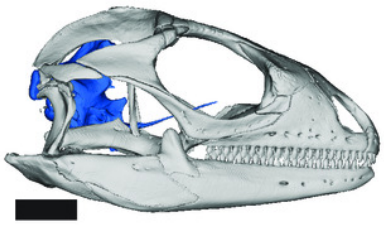

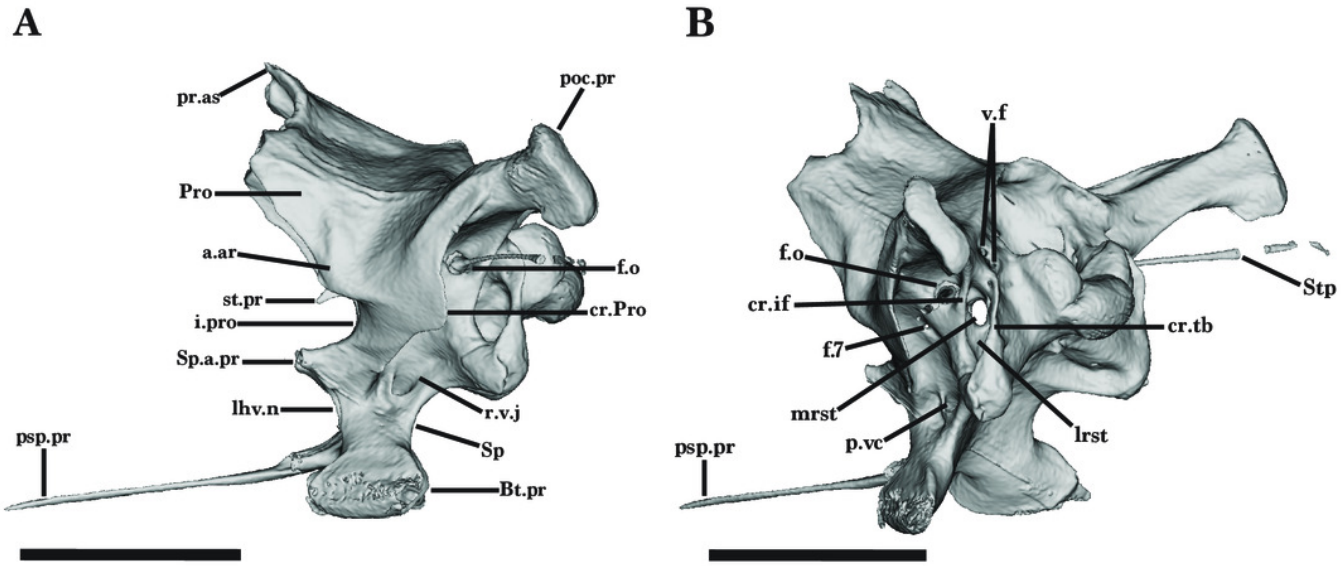
A
pr.as
poc.pr
Pro
a.ar
f.o
st.pr
cr.Pro
i.pro
Sp.a.pr
lhv.n
r.v.j
psp.pr
Sp
Bt.pr
B
v.f
f.o
Stp
cr.if
cr.tb
f.7
mrst
p.vc
lrst
psp.pr

Figure 22

Trachea

Trachea of Cyclura carinata UF Herp 32820 in posterolateral view. Scale bar = 10 mm.

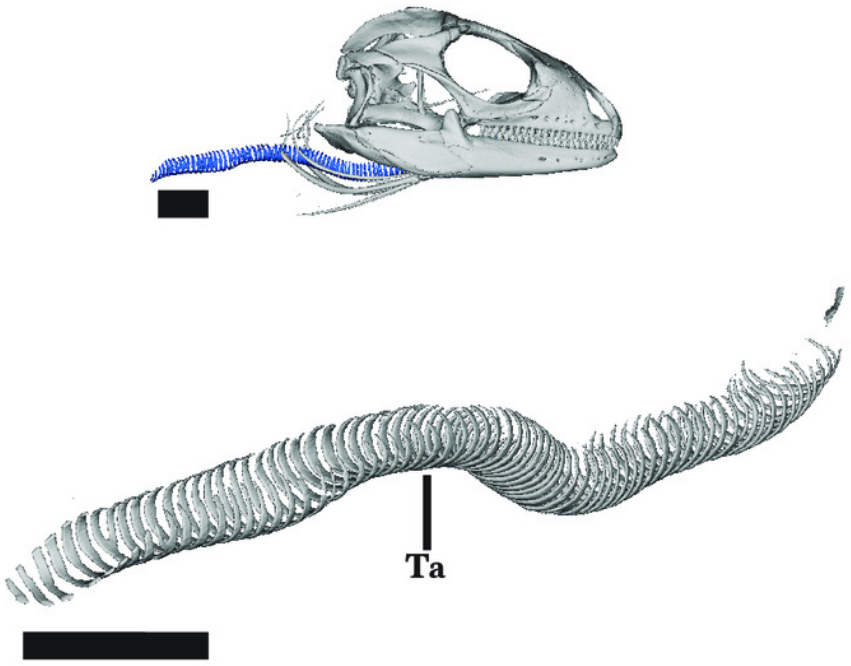

Figure 23

Hyoid

Hyoid of Cyclura carinata UF Herp 32820. A lateral view, B ventral view. Scale bar = 10 mm.

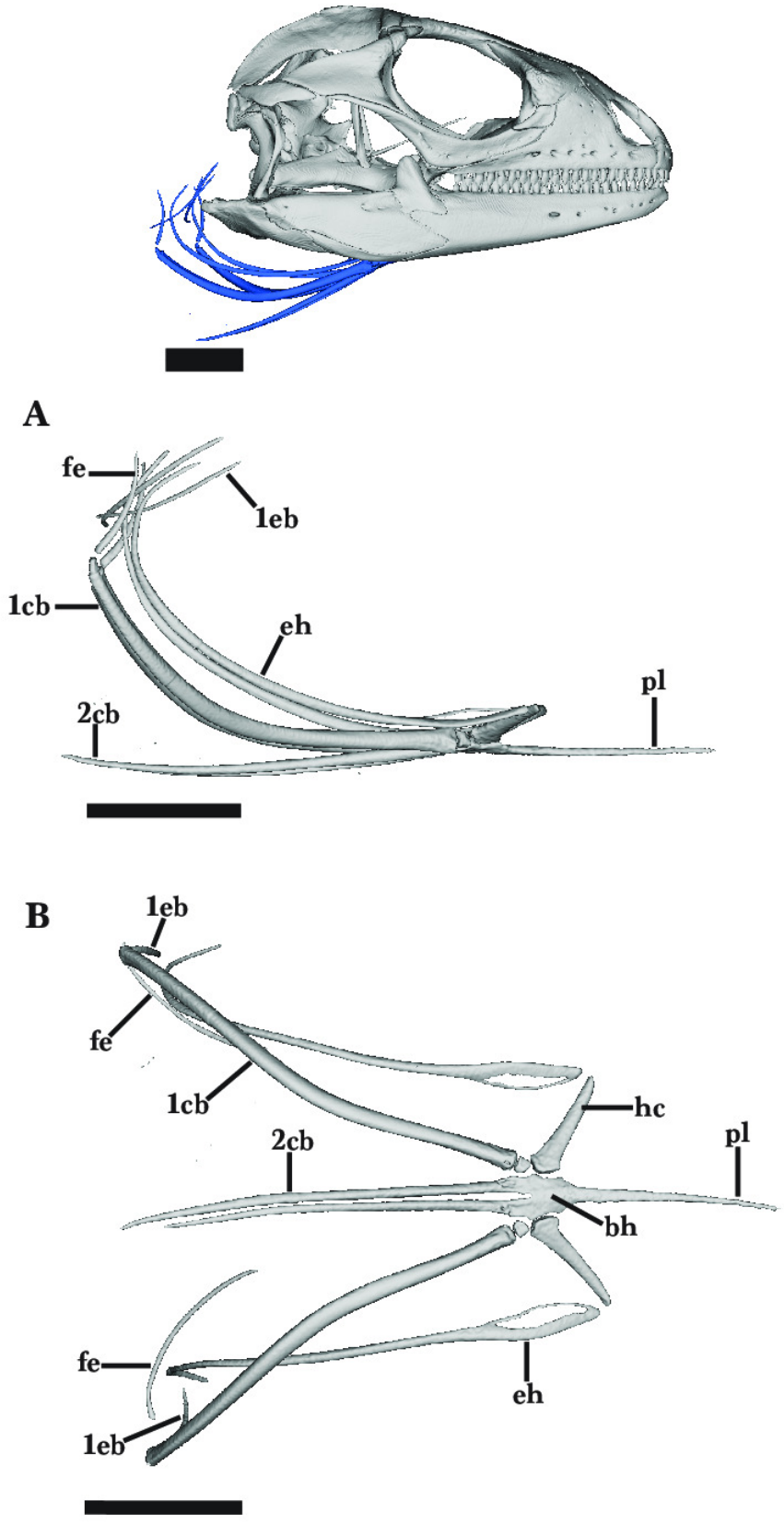
A
fe
1eb
1cb
eh
pl
2cb
B
1eb
fe
1cb
hc
2cb
pl
bh
fe
eh
1eb